

Higher-order mean velocity profile in the convective atmospheric boundary layer

Chenning Tong [†] Davoud Pourabdollah, Kirill Barskov and Mengjie Ding

Department of Mechanical Engineering, Clemson University, Clemson, SC 29634, USA

(Received 17 February 2026)

The higher-order mean velocity profile in the convective atmospheric boundary layer (CBL) is derived using the method of matched asymptotic expansions. The universal expansion coefficients are obtained using field measurement data. The profile accounts for the departures from the (leading-order) log law and local-free-convection scaling as well as the deviations from the Monin-Obukhov Similarity theory (MOST). Invoking MOST and the Multipoint Monin-Obukhov similarity theory, the perturbation equations are obtained from the Reynolds-stress, potential-temperature flux and potential temperature-variance budget equations and the mean momentum and mean potential temperature equations. The small parameters with the most impact in the equations are $(-z_i/L)^{-4/3}$, $(-z_i/L)^{-2/3}$ and $-h_0/L$, where z_i , L and h_0 are the inversion height, the Obukhov length and the roughness height, respectively. Tong and Ding (*J. Fluid Mech.* 2020) have identified the three-layer structure of the CBL with two matching (overlapping) layers, and obtained the leading-order expansions (the local-free-convection scaling and the log law) and the corresponding scales. In the present work, asymptotic matching between the outer and inner-outer layers also results in higher-order expansion terms, which account for the deviations from the local-free-convection scaling and the dependence on z_i/L . Asymptotic matching between the inner-outer and inner-inner layers also results in higher-order expansions that account for the deviations from the log law and the dependence on h_0/L . The expansion coefficients are obtained using measurement data from the recent M²HATS field campaign. Comparisons between the expansions and the measurement show excellent agreement. The higher-order asymptotic expansions show that the convective logarithmic friction law derived by Tong and Ding (2020) is valid to at least the second order. The predicted friction law also agrees well with measurements. The higher-order mean velocity profile can provide improved accuracy over empirical profiles.

[†] Email address for correspondence: ctong@clemson.edu

1. Introduction

The mean velocity profile is an important property characterising the atmospheric boundary layer (ABL). It is also important for a wide range of practical applications such as friction drag (e.g., Kazanski & Monin 1960; Tong & Ding 2020), transport of species and particulates (e.g., Tennekes & Lumley 1972), numerical weather prediction (e.g., Warner 2010) and wind energy (e.g., Wolfson 2012). The Monin-Obukhov similarity theory (MOST, Obukhov 1946; Monin & Obukhov 1954) predicts that the non-dimensional mean shear in the surface layer depends only on $-z/L$, where z is the distance from the surface and $L = -\frac{u_*^3}{\kappa(g/\Theta)Q}$ is the Obukhov length. The other parameters are the friction velocity u_* , the von Kármán constant κ , gravity g , the mean potential temperature Θ , and the surface heat flux Q . The theory is valid asymptotically, i.e., for $z \gg h_0$ and $z_i \gg -L$. The theory also predicts that for $h_0 \ll z \ll -L$ the log law (von Kármán 1930) is recovered and that for $-L \ll z \ll z_i$ the local-free-convection scaling (Wyngaard *et al.* 1971) is predicted, both being the leading-order scaling.

Numerous measurements since the Kansas field campaign (e.g., Businger *et al.* 1971; Wyngaard *et al.* 1971; Kaimal *et al.* 1976; Högström 1988, 1996; Andreas *et al.* 2006) have shown that the mean velocity profile can be approximately described by MOST. However, the theory does not predict the dependence of the mean profile on z/L , i.e., the departures from the leading-order scaling when $z \sim -L$, which must be determined empirically, not from the governing equations. In addition, measurements also show deviations from the MOST profile (i.e., the MOST-scaled profiles do not collapse) that cannot be explained by measurement uncertainties (e.g., Högström 1996; Khanna & Brasseur 1997; Johansson *et al.* 2001; Salesky & Chamecki 2012). The method of matched asymptotic expansions (e.g., Bender & Orszag 1978), which is based on the governing equations, can be employed to systematically predict the dependence on z/L and the deviations from the MOST scaling. We provide a brief description of the method in the following.

A turbulent boundary layer can be mathematically represented as a so-called singular perturbation problem. A shear-driven turbulent boundary layer has two scaling layers (e.g., Panton 2005). The boundary layer equations can be non-dimensionalised using the outer-layer parameters (z_i and u_*) and the inner-layer parameters (ν and u_* for a

smooth surface) to obtain the outer and inner perturbation equations respectively, which contain small (perturbation) parameters, such as the inverse of the friction Reynolds number. The solution of the outer and inner equations can be written as outer and inner asymptotic expansions respectively. However, The outer-layer solution (the velocity defect, von Kármán 1930) cannot be extended to the surface while the inner-layer solution (the law of the wall, Prandtl 1925) cannot be extended to the outer layer. In particular, the leading-order solution for the outer equations or the inner equations (i.e., when the small parameters are set to zero) is qualitatively different from the solution of the equations for the entire boundary layer (i.e., when the parameters are small but non-zero), indicating that the zero-parameter point is singular in the parameter space, hence the term singular perturbation (Bender & Orszag 1978). Asymptotic matching of the leading-order solutions results in the log law. Deviations from the log law in the matching layer can be accounted for using the higher-order terms in the asymptotic expansions.

The convective boundary layer has a three layer structure (Tong & Ding 2020). The non-dimensional boundary layer (perturbation) equations contain small parameters, such as $(-z_i/L)^{-2/3}$ and $-h_0/L$. In the outer layer ($z \sim z_i$), which includes the mixed layer, the mean velocity profile is in the form of the mixed-layer defect law (Tong & Ding 2020). There are two inner scaling layers, both in the surface layer ($z \ll z_i$). In the inner-outer layer ($z \sim -L \ll z_i$), the mean velocity profile is in the form of the surface-layer defect law (Tong & Ding 2020). This layer is the MOST layer with the leading-order non-dimensional mean shear being only a function of z/L . In the inner-inner layer the leading-order profile is given as the law of the wall (Prandtl 1925). Asymptotically matching the leading-order outer and inner-outer expansions leads to the local-free-convection scaling, while asymptotically matching the inner-outer and inner-inner expansions leads to the log law. Similar to the neutral boundary layers, deviations from the leading-order scaling can be accounted for using higher-order expansions. This method not only can identify the additional parameters that influence the mean profile, but also can quantify their influences, including the functional form. Therefore, higher-order asymptotic expansions provide an effective approach to systematically account for the influences of the additional parameters. Note that $(-z_i/L)^{-2/3}$ and $-h_0/L$ are not MOST parameters, indicating

that the higher-order expansions do not follow the MOST scaling, which is a leading-order prediction. Several previous studies (e.g., Khanna & Brasseur 1997; Salesky & Chamecki 2012) have suggested inclusion of z_i/L as an additional parameter based on dimensional analysis. However, dimensional analysis cannot determine the relative importance of the parameters and the functional dependence of the velocity profile on them.

In the present study, we extend the asymptotic expansion analysis of Tong & Ding (2020) by deriving the higher-order expansions of the streamwise mean velocity profile in the convective boundary layer, which provide corrections to the leading-order mean velocity profile. The analysis is based on both the MOST and the MMO scaling. The predicted scaling of the higher-order terms are validated and the non-dimensional expansions coefficients are quantified using field measurements from the Multipoint Monin-Obukhov Similarity Horizontal Array Turbulence Study (M²HATS) field campaign (Tong *et al.* 2026). The higher-order expansions not only provide new insights into the structure and scaling of the CBL, but also improve the quantitative characterization of the mean velocity profile.

In Section 2, we derive the perturbation equations governing the outer, inner-outer, and inner-inner layers, and formally express the mean velocity profile as asymptotic expansions. We then perform higher-order asymptotic matching between the outer and inner-outer layer expansions, as well as between the inner-outer and inner-inner layer expansions. Section 3 describes the procedures for determining the expansion coefficients using field measurements. In Section 4, we present the resulting expansion coefficients and validate the asymptotic expansions through comparison with the field data. Section 5 concludes with a summary of the main findings and their implications. Details of the procedures involved in the determination of the expansion coefficients are provided in the appendices.

2. Perturbation equations

Here we obtain the perturbation equations for the three layers in the CBL. The starting point is the shear-stress budget equations, the vertical temperature flux budget equation, the mean momentum and mean potential temperature equations, and the velocity and

temperature variance budget equations (Wyngaard 2010)

$$\frac{\partial \overline{uw}}{\partial t} + \overline{w^2} \frac{\partial U}{\partial z} - \frac{g}{T} \overline{u\theta} + \overline{\frac{\partial uw^2}{\partial z}} + \overline{u \frac{\partial p}{\partial z}} + \overline{w \frac{\partial p}{\partial x}} + 2(\Omega_2 \overline{w^2} + \Omega_1 \overline{uv} - \Omega_3 \overline{vw} - \Omega_2 \overline{u^2}) = 0, \quad (2.1)$$

$$\frac{\partial \overline{vw}}{\partial t} + \overline{w^2} \frac{\partial V}{\partial z} - \frac{g}{T} \overline{v\theta} + \overline{\frac{\partial vw^2}{\partial z}} + \overline{v \frac{\partial p}{\partial z}} + \overline{w \frac{\partial p}{\partial y}} + 2(\Omega_1 \overline{v^2} + \Omega_3 \overline{uw} - \Omega_1 \overline{w^2} - \Omega_2 \overline{uv}) = 0, \quad (2.2)$$

$$\frac{\partial \overline{w\theta}}{\partial t} + \overline{w^2} \frac{\partial \Theta}{\partial z} + \overline{\frac{\partial w^2\theta}{\partial z}} + \overline{\theta \frac{\partial p}{\partial z}} + 2(\Omega_1 \overline{v\theta} - \Omega_2 \overline{u\theta}) + \frac{g}{T} \overline{\theta^2} = 0, \quad (2.3)$$

$$\frac{\partial \overline{vw}}{\partial z} = f(U_g - U) + \frac{d\tau_{ry}}{dz}, \quad (2.4)$$

$$\frac{\partial \overline{uw}}{\partial z} = f(V - V_g) + \frac{d\tau_{rx}}{dz}, \quad (2.5)$$

$$\frac{\partial \Theta}{\partial t} + \frac{\partial \overline{w\theta}}{\partial z} = 0, \quad (2.6)$$

$$\frac{1}{2} \frac{\partial \overline{w^2}}{\partial t} = -\frac{1}{2} \frac{\partial \overline{w^3}}{\partial z} + \overline{p \frac{\partial w}{\partial z}} - \overline{\frac{\partial pw}{\partial z}} + \frac{g}{T} \overline{w\theta} - \varepsilon_3, \quad (2.7)$$

$$\frac{1}{2} \frac{\partial \overline{u^2}}{\partial t} = -\overline{uw} \frac{\partial U}{\partial z} - \frac{1}{2} \frac{\partial \overline{wu^2}}{\partial z} + \overline{p \frac{\partial u}{\partial x}} - \varepsilon_1, \quad (2.8)$$

$$\frac{1}{2} \frac{\partial \overline{\theta^2}}{\partial t} = -\overline{w\theta} \frac{\partial \Theta}{\partial z} - \frac{1}{2} \frac{\partial \overline{w\theta^2}}{\partial z} - \varepsilon_\theta, \quad (2.9)$$

where $\Omega_i s$, $f = 2\Omega_3$, τ_{rx} , τ_{ry} , ε_1 , ε_3 , and ε_θ are the components of Earth's rotation vector, Coriolis parameter, the shear-stress in the x- and y-directions induced by the surface roughness, dissipation rates for $\overline{u^2}/2$, $\overline{w^2}/2$, and $\overline{\theta^2}/2$, respectively. The viscous terms except the dissipation rates in the variance budgets are neglected. The Coriolis terms in (2.1), (2.2) and (2.3) are of higher order (e.g., Wyngaard 2010), thus we neglect them in this analysis. In the following we derive the perturbation equations in the different scaling layers.

2.1. Outer layer

We first derive the the outer-layer (the mixed layer) equations. We use U_m , V_g , z_i , u_*^2 , $u_*^2 w_e / (f z_i) = V_g w_e$, w_*^2 , Q , and z_i / w_* as the outer scales for the mean velocity components, height from the surface, the streamwise and lateral kinematic stress components, velocity variance, potential temperature flux, and time to define the dimensionless outer

variables:

$$\begin{aligned}
U(z) &= U_m U_o \left(\frac{z}{z_i} \right), \quad V(z) = V_g V_o \left(\frac{z}{z_i} \right), \quad \Theta = \Theta_m \Theta_o \left(\frac{z}{z_i} \right), \quad \overline{uw} = u_*^2 \overline{uw}_o, \quad \overline{vw} = \frac{u_*^2 w_e}{f z_i} \overline{vw}_o, \\
z &= z_i z_o, \quad \overline{u\theta} = Q \overline{u\theta}_o, \quad t = \frac{z_i}{w_*} \tau, \quad \overline{w^2} = w_*^2 \overline{w_o^2}, \quad \overline{u^2} = w_*^2 \overline{u_o^2}, \quad \overline{w\theta} = Q \overline{w\theta}_o, \quad \overline{\theta^2} = \left(\frac{Q}{w_*} \right)^2 \overline{\theta_o^2}, \\
p &= w_*^2 p_o,
\end{aligned} \tag{2.10}$$

where w_* and w_e are the mixed-layer velocity scale and the entrainment velocity (at the capping inversion), respectively. The scales of most of the terms are obtained using MOST and the mixed-layer scaling, while the others, e.g., the velocity–pressure-gradient correlation, are obtained using the spectral scaling obtained using MMO (Tong & Ding 2019). Substituting the outer variables given in (2.10) into equations (2.1) to (2.9) we obtain

$$\frac{\partial \overline{uw}_o}{\partial \tau} \frac{u_*^2 w_*}{z_i} + w_*^2 \overline{w_o^2} \frac{U_m}{z_i} \frac{\partial U_o}{\partial z_o} - \frac{g}{T} Q \overline{u\theta}_o + \frac{w_* u_*^2}{z_i} \left(\frac{\partial \overline{uw}^2}_o + \left(\overline{u \frac{\partial p}{\partial z}} \right)_o + \left(\overline{w \frac{\partial p}{\partial x}} \right)_o \right) = 0. \tag{2.11}$$

$$\frac{\partial \overline{vw}_o}{\partial \tau} \frac{u_*^2 w_e}{f z_i} \frac{w_*}{z_i} + w_*^2 \overline{w_o^2} \frac{V_g}{z_i} \frac{\partial V_o}{\partial z_o} - \frac{g}{T} Q \overline{v\theta}_o + \frac{w_*}{z_i} \frac{u_*^2 w_e}{f z_i} \left(\frac{\partial \overline{vw}^2}_o + \left(\overline{v \frac{\partial p}{\partial z}} \right)_o + \left(\overline{w \frac{\partial p}{\partial y}} \right)_o \right) = 0, \tag{2.12}$$

$$\frac{\partial \overline{w\theta}_o}{\partial \tau} \frac{Q w_*}{z_i} + w_*^2 \overline{w_o^2} \frac{\partial \Theta_o}{\partial z_o} \frac{\Theta_m}{z_i} + \frac{Q w_*}{z_i} \left(\frac{\partial \overline{w^2\theta}_o}{\partial z_o} + \left(\overline{\theta \frac{\partial p}{\partial z}} \right)_o \right) + \frac{g}{T} \left(\frac{Q}{w_*} \right)^2 \overline{\theta_o^2} = 0, \tag{2.13}$$

$$\frac{u_*^2}{z_i} \frac{\partial \overline{uw}_o}{\partial z_o} = f V_g (V_o - 1), \tag{2.14}$$

$$\frac{u_*^2 w_e}{f z_i} \frac{1}{z_i} \frac{\partial \overline{vw}_o}{\partial z_o} = f U_m \frac{U_g - U}{U_m}, \quad \text{with } U_m \equiv U_g - \frac{u_*^2 w_e}{f^2 z_i^2}. \tag{2.15}$$

$$\frac{\Theta_m}{z_i / w_*} \frac{\partial \Theta_o}{\partial \tau} + \frac{Q}{z_i} \frac{\partial \overline{w\theta}_o}{\partial z_o} = 0, \tag{2.16}$$

$$\frac{1}{2} \frac{w_*^2}{z_i / w_*} \frac{\partial \overline{w_o^2}}{\partial \tau} = -\frac{1}{2} \frac{w_*^3}{z_i} \frac{\partial \overline{w_o^3}}{\partial z_o} + \frac{w_*^3}{z_i} \left(\overline{p \frac{\partial w}{\partial z}} \right)_o - \frac{w_*^3}{z_i} \left(\overline{\frac{\partial p w}{\partial z}} \right)_o + \frac{g}{T} Q \overline{w\theta}_o - \varepsilon_3, \tag{2.17}$$

$$\frac{1}{2} \frac{w_*^2}{z_i / w_*} \frac{\partial \overline{u_o^2}}{\partial \tau} = \frac{w_*^3}{z_i} \left(-\frac{z_i}{L} \right)^{-1/3} \overline{uw}_o \left(\frac{\partial U}{\partial z} \right)_o - \frac{1}{2} \frac{w_*^3}{z_i} \frac{\partial \overline{wu_o^2}}{\partial z_o} + \frac{w_*^3}{z_i} \left(\overline{p \frac{\partial u}{\partial x}} \right)_o - \varepsilon_1, \tag{2.18}$$

$$\frac{1}{2} \left(\frac{Q}{w_*} \right)^2 \frac{w_*}{z_i} \frac{\partial \overline{\theta_o^2}}{\partial \tau} = -Q \frac{Q}{w_* z_i} \overline{w\theta}_o \left(\frac{\partial \Theta}{\partial z} \right)_o - \frac{1}{2} \left(\frac{Q}{w_*} \right)^2 \frac{w_*}{z_i} \frac{\partial \overline{w\theta^2}_o}{\partial z_o} - \varepsilon_\theta. \tag{2.19}$$

Using $w_*^2 U_m / z_i$, $Q w_* / z_i$, u_*^2 / z_i , $\Theta_m w_*^2 / z_i$, w_*^3 / z_i and $Q^2 / w_* z_i$ to non-dimensionalise the shear-stress and vertical flux budgets, the mean momentum and mean potential temper-

ature equations, and the variance budgets respectively, we obtain the outer equations

$$\epsilon_1 \frac{\partial \bar{u}w_o}{\partial \tau} + \bar{w}_o^2 \frac{\partial U_o}{\partial z_o} - \frac{w_*}{U_m} \bar{u} \theta_o + \epsilon_1 \left(\frac{\partial \bar{u}w_o^2}{\partial z_o} + \left(\bar{u} \frac{\partial p}{\partial z} \right)_o + \left(\bar{w} \frac{\partial p}{\partial x} \right)_o \right) = 0, \quad (2.20)$$

$$\epsilon_2 \frac{V_g}{U_m} \frac{\partial \bar{v}w_o}{\partial \tau} + \bar{w}_o^2 \frac{V_g}{U_m} \frac{\partial V_o}{\partial z_o} - \frac{w_*}{U_m} \bar{v} \theta_o + \epsilon_2 \frac{V_g}{U_m} \left(\frac{\partial \bar{v}w_o^2}{\partial z_o} + \left(\bar{v} \frac{\partial p}{\partial z} \right)_o + \left(\bar{w} \frac{\partial p}{\partial y} \right)_o \right) = 0, \quad (2.21)$$

$$\epsilon_\theta \frac{\partial \bar{w} \theta_o}{\partial \tau} + \bar{w}_o^2 \frac{\partial \Theta_o}{\partial z_o} + \epsilon_\theta \left(\frac{\partial \bar{w}^2 \theta_o}{\partial z_o} + \left(\bar{\theta} \frac{\partial p}{\partial z} \right)_o \right) + \epsilon_\theta \bar{\theta}_o^2 = 0, \quad (2.22)$$

$$\frac{\partial \bar{u}w_o}{\partial z_o} = -V_o + 1 = 1 - \epsilon_2 V_{o,2}, \quad (2.23)$$

$$\frac{\partial \bar{v}w_o}{\partial z_o} = 1 - \epsilon_4 U_{o,2}. \quad (2.24)$$

$$\frac{\partial \Theta_o}{\partial \tau} + \epsilon_\theta \frac{\partial \bar{w} \theta_o}{\partial z_o} = 0, \quad (2.25)$$

$$\frac{1}{2} \frac{\partial \bar{w}_o^2}{\partial \tau} = -\frac{1}{2} \frac{\partial \bar{w}_o^3}{\partial z_o} + \left(\bar{p} \frac{\partial \bar{w}}{\partial z} \right)_o - \left(\bar{p} \frac{\partial \bar{w} \bar{u}}{\partial z} \right)_o + \bar{w} \theta_o - \varepsilon_{3o}, \quad (2.26)$$

$$\frac{1}{2} \frac{\partial \bar{u}_o^2}{\partial \tau} = -\epsilon_3 \bar{u} \bar{w}_o \left(\frac{\partial U}{\partial z} \right)_o - \frac{1}{2} \frac{\partial \bar{w} \bar{u}_o^2}{\partial z_o} + \left(\bar{p} \frac{\partial \bar{u}}{\partial x} \right)_o - \varepsilon_{1o}, \quad (2.27)$$

$$\frac{1}{2} \frac{\partial \bar{\theta}_o^2}{\partial \tau} = -\bar{w} \theta_o \left(\frac{\partial \Theta}{\partial z} \right)_o - \frac{1}{2} \frac{\partial \bar{w} \bar{\theta}_o^2}{\partial z_o} - \varepsilon_{\theta o} \quad (2.28)$$

The small parameters in the outer equations are

$$\epsilon_1 = \frac{u_*}{w_*} \frac{u_*}{U_m}, \quad \epsilon_2 = \frac{w_e}{w_*}, \quad \epsilon_3 = (-\frac{z_i}{L})^{-4/3}, \quad \epsilon_4 = \epsilon_1 U_m / \frac{V_g w_e}{f z_i}, \quad \epsilon_\theta = \frac{Q}{w_* \Theta_m}. \quad (2.29)$$

Here ϵ_1 is the relative scale of the velocity defect to the mean velocity in the outer layer and ϵ_3 quantifies the influence of the shear production of \bar{u}^2 . In the outer layer, $z > -L$, therefore the shear production is a small term. ϵ_2 and ϵ_4 quantify the influence of entrainment and the Coriolis force on the U - and V -components of the mean velocity. ϵ_θ is the relative scale of the potential temperature defect relative to the difference of the mixed-layer mean temperature and surface mean temperature. With these small parameters, the outer solution can be written as the following outer asymptotic expansions

$$U_o = U_{o,1} + \epsilon_1 U_{o,2} + \epsilon_1 \epsilon_3 U_{o,31} + \epsilon_1 \epsilon_2 U_{o,32} + \dots, \quad (2.30)$$

$$\bar{w}_o^2(z_o) = \bar{w}_{o,1}^2(z_o) + \epsilon_3 \bar{w}_{o,2}^2(z_o) + O(\epsilon_3^2), \quad (2.31)$$

$$\frac{\partial \bar{u}w_o^2}{\partial z_o} = \frac{\partial \bar{u}w_{o,1}^2}{\partial z_o} + \epsilon_3 \frac{\partial \bar{u}w_{o,21}^2}{\partial z_o} + \epsilon_2 \frac{\partial \bar{u}w_{o,22}^2}{\partial z_o} + \dots, \quad (2.32)$$

$$\frac{\partial \bar{u}w_o}{\partial z_o} = \frac{\partial \bar{u}w_{o,1}}{\partial z_o} + \epsilon_3 \frac{\partial \bar{u}w_{o,21}}{\partial z_o} + \epsilon_2 \frac{\partial \bar{u}w_{o,22}}{\partial z_o} + \dots, \quad (2.33)$$

$$V_o = V_{o,1} + \epsilon_2 V_{o,2} + \epsilon_2 \epsilon_3 V_{o,31} + \epsilon_2 \epsilon_4 V_{o,32} + \dots, \quad (2.34)$$

$$\frac{\partial \overline{vw^2}_o}{\partial z_o} = \frac{\partial \overline{vw^2}_{o,1}}{\partial z_o} + \epsilon_3 \frac{\partial \overline{vw^2}_{o,21}}{\partial z_o} + \epsilon_4 \frac{\partial \overline{vw^2}_{o,22}}{\partial z_o} + \dots, \quad (2.35)$$

$$\frac{\partial \overline{vw}_o}{\partial z_o} = \frac{\partial \overline{vw}_{o,1}}{\partial z_o} + \epsilon_3 \frac{\partial \overline{vw}_{o,21}}{\partial z_o} + \epsilon_4 \frac{\partial \overline{vw}_{o,22}}{\partial z_o} + \dots. \quad (2.36)$$

$$\Theta_o = \Theta_{o,1} + \epsilon_\theta \Theta_{o,2} + \epsilon_\theta \epsilon_3 \Theta_{o,3} + \dots, \quad (2.37)$$

Substituting the outer expansions back to equations (2.20), (2.26) and (2.27) we obtain

$$\begin{aligned} \epsilon_1 \frac{\partial \overline{uw}_o}{\partial \tau} + \left(\overline{w_{o,1}^2} + \epsilon_3 \overline{w_{o,2}^2} + \dots \right) \left(\frac{\partial U_{o,1}}{\partial z_o} + \epsilon_1 \frac{\partial U_{o,2}}{\partial z_o} + \epsilon_1 \epsilon_3 \frac{\partial U_{o,31}}{\partial z_o} + \epsilon_1 \epsilon_2 \frac{\partial U_{o,32}}{\partial z_o} + \dots \right) \\ + \dots + \epsilon_1 \left(\left(\overline{w \frac{\partial p}{\partial x}} \right)_{o,1} + \epsilon_3 \left(\overline{w \frac{\partial p}{\partial x}} \right)_{o,2} + \epsilon_2 \left(\overline{w \frac{\partial p}{\partial x}} \right)_{o,3} + \dots \right) = 0. \end{aligned} \quad (2.38)$$

$$\begin{aligned} \frac{1}{2} \left(\frac{\partial \overline{w_{o,1}^2}}{\partial \tau} + \epsilon_3 \frac{\partial \overline{w_{o,2}^2}}{\partial \tau} + \dots \right) = -\frac{1}{2} \left(\frac{\partial \overline{w_{o,1}^3}}{\partial z_o} + \epsilon_3 \frac{\partial \overline{w_{o,2}^3}}{\partial z_o} + \dots \right) + \dots \\ + \left(\overline{w \theta}_{o,1} + \epsilon_\theta \overline{w \theta}_{o,2} + \dots \right) - \epsilon_{3o} \end{aligned} \quad (2.39)$$

$$\begin{aligned} \frac{1}{2} \frac{\partial \overline{u_o^2}}{\partial \tau} = -\epsilon_3 \left(\overline{uw}_{o,1} + \epsilon_3 \overline{uw}_{o,2} + \epsilon_2 \overline{uw}_{o,3} + \dots \right) \left(\frac{\partial U_{o,1}}{\partial z_o} + \epsilon_1 \frac{\partial U_{o,2}}{\partial z_o} + \epsilon_1 \epsilon_3 \frac{\partial U_{o,31}}{\partial z_o} \right. \\ \left. + \epsilon_1 \epsilon_2 \frac{\partial U_{o,32}}{\partial z_o} + \dots \right) - \frac{1}{2} \left(\frac{\partial \overline{uw^2}_{o,1}}{\partial z_o} + \epsilon_3 \frac{\partial \overline{uw^2}_{o,21}}{\partial z_o} + \epsilon_2 \frac{\partial \overline{uw^2}_{o,22}}{\partial z_o} + \dots \right) + \dots - \epsilon_{1o} \end{aligned} \quad (2.40)$$

It can be seen that the second-order mean velocity gradient is induced by the second-order pressure–velocity-gradient interaction term, which is in turn induced by the mean shear production of $\overline{u_o^2}$. The last term is of second order in the outer layer, but becomes leading order for $-z/L \sim 1$, and therefore is the source of the singularity for the outer equations.

2.2. Inner-outer layer

Due to the mean shear production term being of leading order for $z \sim -L$, the leading-order outer solution is no longer valid, indicating that there exists an inner scaling layer there (Tong & Ding 2020). In fact, there are two inner layers, the inner-outer layer with a thickness of $-L$ and the inner-inner layer with a thickness of h_0 . We define the

	ϵ_1	ϵ_2	ϵ_3	ϵ_4	—	ϵ_θ
Outer layer	$\frac{u_*}{w_*} \frac{u_*}{U_m}$	$\frac{w_e}{w_*}$	$(-\frac{z_i}{L})^{-\frac{4}{3}}$	$\frac{\epsilon_1 U_m}{V_g w_e / fz_i}$	—	$\frac{Q}{w_* \Theta_m}$
Inner-outer layer	ϵ'_1	ϵ'_2	ϵ'_3	ϵ'_4	ϵ'_5	ϵ'_θ
	$\frac{u_*}{U_m}$	$\frac{u_*^2}{w_*^2} \frac{w_e}{w_*}$	$(-\frac{z_i}{L})^{-\frac{2}{3}}$	$\frac{\epsilon'_1 U_m}{V_g w_e / fz_i}$	$\frac{L}{z_i}$	$\frac{Q}{u_* \Theta_m}$
Inner-inner layer	ϵ'_1	ϵ''_2	ϵ''_3	ϵ''_4	ϵ''_5	ϵ'_θ
	$\frac{u_*}{U_m}$	$\frac{f h_0}{u_*} \frac{U_g}{V_g}$	$\frac{h_0}{L}$	$\frac{u_*}{U_g}$	$\frac{h_0}{z_i}$	$\frac{Q}{u_* \Theta_m}$

Table 1: Small parameters in the perturbation equations.

non-dimensional inner-outer variables as

$$\begin{aligned}
U(z) &= U_m U_{io}(-\frac{z}{L}), \quad V(z) = V_g V_{io}(-\frac{z}{L}), \quad \Theta = \Theta_m \Theta_{io}(-\frac{z}{L}), \quad \overline{uw} = u_*^2 \overline{uw}_{io}, \\
\overline{vw} &= \frac{u_*^2 w_e}{fz_i} (-\frac{L}{z_i}) \overline{vw}_{io}, \quad z = -L z_{io}, \quad \overline{u\theta} = Q \overline{u\theta}_{io}, \quad t = \frac{z_i}{w_*} \tau, \quad \overline{w^2} = u_*^2 \overline{w^2}_{io}, \quad \overline{u^2} = u_*^2 \overline{u^2}_{io}, \\
\overline{w\theta} &= Q \overline{w\theta}_{io}, \quad \overline{\theta^2} = (\frac{Q}{u_*})^2 \overline{\theta^2}_{io}, \quad p = u_*^2 p_{io},
\end{aligned} \tag{2.41}$$

Substituting the variables given in (2.41) into equations (2.1) to (2.9) we obtain

$$\frac{u_*^2 w_*}{z_i} \frac{\partial \overline{uw}_{io}}{\partial \tau} + u_*^2 \overline{w^2}_{io} \frac{U_m}{-L} \frac{\partial U_{io}}{\partial z_{io}} - \frac{g}{T} Q \overline{u\theta}_{io} + \frac{u_*^3}{-L} \left(\frac{\partial \overline{uw^2}_{io}}{\partial z_{io}} + \left(\overline{w} \frac{\partial \overline{p}}{\partial x} \right)_{io} + \left(\overline{u} \frac{\partial \overline{p}}{\partial z} \right)_{io} \right) = 0, \tag{2.42}$$

$$\frac{u_*^2 w_e}{fz_i} \left(-\frac{L}{z_i} \right) \frac{w_*}{z_i} \frac{\partial \overline{vw}_{io}}{\partial \tau} + u_*^2 \overline{w^2}_{io} \frac{V_g}{-L} \frac{\partial V_{io}}{\partial z_{io}} - \frac{g}{T} Q \overline{v\theta}_{io} + \frac{u_*}{z_i} \frac{u_*^2 w_e}{fz_i} \left(\frac{\partial \overline{vw^2}_{io}}{\partial z_{io}} + \left(\overline{w} \frac{\partial \overline{p}}{\partial y} \right)_{io} + \left(\overline{v} \frac{\partial \overline{p}}{\partial z} \right)_{io} \right) = 0, \tag{2.43}$$

$$\frac{Q w_*}{z_i} \frac{\partial \overline{w\theta}_{io}}{\partial \tau} + u_*^2 \overline{w^2}_{io} \frac{\Theta_m}{-L} \frac{\partial \Theta_{io}}{\partial z_{io}} + \frac{g}{T} \left(\frac{Q}{u_*} \right)^2 \overline{\theta^2}_{io} + \frac{Q u_*}{-L} \left(\frac{\partial \overline{w^2\theta}_{io}}{\partial z_{io}} + \left(\overline{\theta} \frac{\partial \overline{p}}{\partial z} \right)_{io} \right) = 0, \tag{2.44}$$

$$\frac{u_*^2}{L} \frac{\partial \overline{uw}_{io}}{\partial z_{io}} = f(V - V_g), \tag{2.45}$$

$$\frac{u_*^2 w_e}{fz_i} \left(-\frac{L}{z_i} \right) \frac{1}{L} \frac{\partial \overline{vw}_{io}}{\partial z_{io}} = f(U_g - U). \tag{2.46}$$

$$\frac{\Theta_m}{z_i/w_*} \frac{\partial \Theta_{io}}{\partial \tau} + \frac{Q}{L} \frac{\partial \overline{w\theta}_{io}}{\partial z_{io}} = 0, \tag{2.47}$$

$$\frac{1}{2} \frac{u_*^2 w_*}{z_i} \frac{\partial \overline{w}_{io}^2}{\partial \tau} = -\frac{1}{2} \frac{\partial \overline{w}_{io}^3}{\partial z_{io}} \frac{u_*^3}{L} + \left(p \frac{\partial \overline{w}}{\partial z} \right)_{io} \frac{u_*^3}{L} - \left(\frac{\partial \overline{p} w}{\partial z} \right)_{io} \frac{u_*^3}{L} + \frac{g}{T} Q \overline{w} \overline{\theta}_{io} - \varepsilon_3, \quad (2.48)$$

$$\frac{1}{2} \frac{u_*^2 w_*}{z_i} \frac{\partial \overline{u}_{io}^2}{\partial \tau} = -\overline{u} \overline{w}_{io} \left(\frac{\partial U}{\partial z} \right)_{io} \frac{u_*^3}{L} - \frac{1}{2} \frac{\partial \overline{w} \overline{u}_{io}^2}{\partial z_{io}} \frac{u_*^3}{L} + \left(p \frac{\partial \overline{u}}{\partial x} \right)_{io} \frac{u_*^3}{L} - \varepsilon_1, \quad (2.49)$$

$$\frac{1}{2} \left(\frac{Q}{u_*} \right)^2 \frac{w_*}{z_i} \frac{\partial \overline{\theta}_{io}^2}{\partial \tau} = -Q \frac{Q}{u_* L} \overline{w} \overline{\theta}_{io} \left(\frac{\partial \Theta}{\partial z} \right)_{io} - \frac{1}{2} \left(\frac{Q}{u_*} \right)^2 \frac{u_*}{L} \frac{\partial \overline{w} \overline{\theta}_{io}^2}{\partial z_{io}} - \varepsilon_\theta. \quad (2.50)$$

Using $u_*^2 U_m / (-L)$, $Q u_* / (-L)$, $u_*^2 / (-L)$, $\Theta_m u_*^2 / (-L)$, $u_*^3 / (-L)$ and $Q^2 / u_* (-L)$ to non-dimensionalise the shear-stress and vertical flux budgets, the mean momentum and mean potential temperature equations, as well as the associated variance budgets, we obtain the corresponding inner-outer equations

$$\epsilon'_1 \epsilon'_3 \frac{\partial \overline{u} \overline{w}_{io}}{\partial \tau} + \overline{w}_{io}^2 \frac{\partial \overline{U}_{io}}{\partial z_{io}} - \epsilon'_1 \overline{u} \overline{\theta}_{io} + \epsilon'_1 \left(\frac{\partial \overline{u} \overline{w}_{io}^2}{\partial z_{io}} + \left(\overline{w} \frac{\partial \overline{p}}{\partial x} \right)_{io} + \left(\overline{u} \frac{\partial \overline{p}}{\partial z} \right)_{io} \right) = 0, \quad (2.51)$$

$$\frac{u_*^4 w_e}{w_*^5} \frac{V_g}{U_m} \frac{\partial \overline{v} \overline{w}_{io}}{\partial \tau} + \overline{w}_{io}^2 \frac{V_g}{U_m} \frac{\partial \overline{V}_{io}}{\partial z_{io}} - \epsilon'_1 \overline{v} \overline{\theta}_{io} + \epsilon'_2 \frac{V_g}{U_m} \left(\frac{\partial \overline{v} \overline{w}_{io}^2}{\partial z_{io}} + \left(\overline{w} \frac{\partial \overline{p}}{\partial y} \right)_{io} + \left(\overline{v} \frac{\partial \overline{p}}{\partial z} \right)_{io} \right) = 0. \quad (2.52)$$

$$\epsilon'_3 \epsilon'_\theta \frac{\partial \overline{w} \overline{\theta}_{io}}{\partial \tau} + \overline{w}_{io}^2 \frac{\partial \overline{\Theta}_{io}}{\partial z_{io}} + \epsilon'_\theta \overline{\theta}_{io}^2 + \epsilon'_\theta \left(\frac{\partial \overline{w}^2 \overline{\theta}_{io}}{\partial z_{io}} + \left(\overline{\theta} \frac{\partial \overline{p}}{\partial z} \right)_{io} \right) = 0, \quad (2.53)$$

$$\frac{\partial \overline{u} \overline{w}_{io}}{\partial z_{io}} = -\epsilon'_5 - \epsilon'_5 \epsilon'_2 V_{io,2} \quad (2.54)$$

$$\frac{\partial \overline{v} \overline{w}_{io}}{\partial z_{io}} = 1 - \epsilon'_4 U_{io,2} \quad (2.55)$$

$$\epsilon'_3 \frac{\partial \overline{\Theta}_{io}}{\partial \tau} + \epsilon'_\theta \frac{\partial \overline{w} \overline{\theta}_{io}}{\partial z_{io}} = 0, \quad (2.56)$$

$$\frac{1}{2} \epsilon'_3 \frac{\partial \overline{w}_{io}^2}{\partial \tau} = -\frac{1}{2} \frac{\partial \overline{w}_{io}^3}{\partial z_{io}} + \left(p \frac{\partial \overline{w}}{\partial z} \right)_{io} - \left(\frac{\partial \overline{p} w}{\partial z} \right)_{io} + \overline{w} \overline{\theta}_{io} - \varepsilon_{3io}, \quad (2.57)$$

$$\frac{1}{2} \epsilon'_3 \frac{\partial \overline{u}_{io}^2}{\partial \tau} = -\overline{u} \overline{w}_{io} \left(\frac{\partial U}{\partial z} \right)_{io} - \frac{1}{2} \frac{\partial \overline{w} \overline{u}_{io}^2}{\partial z_{io}} + \left(p \frac{\partial \overline{u}}{\partial x} \right)_{io} - \varepsilon_{1io}, \quad (2.58)$$

$$\frac{1}{2} \epsilon'_3 \frac{\partial \overline{\theta}_{io}^2}{\partial \tau} = -\overline{w} \overline{\theta}_{io} \frac{\partial \overline{\Theta}_{io}}{\partial z_{io}} - \frac{1}{2} \frac{\partial \overline{w} \overline{\theta}_{io}^2}{\partial z_{io}} - \varepsilon_{\theta io}, \quad (2.59)$$

where

$$\epsilon'_1 = \frac{u_*}{U_m}, \quad \epsilon'_2 = \frac{u_*^2}{w_*^2} \frac{w_e}{w_*}, \quad \epsilon'_3 = -\frac{L}{z_i} \frac{w_*}{u_*} = \kappa^{-\frac{1}{3}} (-\frac{z_i}{L})^{-\frac{2}{3}}, \quad \epsilon'_4 = \frac{U_m}{V_g w_e / f z_i} \epsilon'_1, \quad \epsilon'_5 = \frac{L}{z_i}, \quad \epsilon'_\theta = \frac{Q}{u_* \Theta_m}. \quad (2.60)$$

Here ϵ'_1 is the scale of the velocity defect in the inner-outer layer relative to the mixed-layer mean velocity scale. ϵ'_2 and ϵ'_4 quantify the influence of the entrainment. ϵ'_3 quantifies

the influence of the non-stationarity. ϵ'_5 quantifies the effect of the variations of the shear stress with height (the shear stress is treated as a constant only at the leading order). ϵ'_θ represents the relative scale of the temperature defect.

The inner-outer expansions are

$$\overline{w_{io}^2}(z_{io}) = \overline{w_{io,1}^2}(z_{io}) + \epsilon'_3 \overline{w_{io,2}^2}(z_{io}) + O(\epsilon''_3^2), \quad (2.61)$$

$$U_{io} = U_{io,1} + \epsilon'_1 U_{io,2} + \epsilon'_1 \epsilon'_3 U_{io,31} + \epsilon'_1 \epsilon'_5 U_{io,32} + \dots \quad (2.62)$$

$$\frac{\partial \overline{uw_{io}^2}}{\partial z_{io}} = \frac{\partial \overline{uw_{io,1}^2}}{\partial z_{io}} + \epsilon'_3 \frac{\partial \overline{uw_{io,2}^2}}{\partial z_{io}} + \epsilon'_5 \epsilon'_2 \frac{\partial \overline{uw_{io,3}^2}}{\partial z_{io}} + \dots \quad (2.63)$$

$$\frac{\partial \overline{uw_{io}}}{\partial z_{io}} = \frac{\partial \overline{uw_{io,1}}}{\partial z_{io}} + \epsilon'_3 \frac{\partial \overline{uw_{io,2}}}{\partial z_{io}} + \epsilon'_5 \epsilon'_2 \frac{\partial \overline{uw_{io,3}}}{\partial z_{io}} + \dots \quad (2.64)$$

$$V_{io} = V_{io,1} + \epsilon'_2 V_{io,2} + \epsilon'_2 \epsilon'_3 V_{io,31} + \epsilon'_2 \epsilon'_4 V_{io,32} + \dots \quad (2.65)$$

$$\frac{\partial \overline{vw_{io}^2}}{\partial z_{io}} = \frac{\partial \overline{vw_{io,1}^2}}{\partial z_{io}} + \epsilon'_3 \frac{\partial \overline{vw_{io,21}^2}}{\partial z_{io}} + \epsilon'_4 \frac{\partial \overline{vw_{io,22}^2}}{\partial z_{io}} + \dots \quad (2.66)$$

$$\frac{\partial \overline{vw_{io}}}{\partial z_{io}} = \frac{\partial \overline{vw_{io,1}}}{\partial z_{io}} + \epsilon'_3 \frac{\partial \overline{vw_{io,21}}}{\partial z_{io}} + \epsilon'_4 \frac{\partial \overline{vw_{io,22}}}{\partial z_{io}} + \dots \quad (2.67)$$

$$\Theta_{io} = \Theta_{io,1} + \epsilon'_\theta \Theta_{io,2} + \epsilon'_\theta \epsilon'_3 \Theta_{io,3} + \dots, \quad (2.68)$$

Substitute the inner-outer expansions back to equations (2.51), (2.57) and (2.58) we obtain

$$\begin{aligned} & \epsilon'_1 \epsilon'_3 \frac{\partial \overline{uw_{io}}}{\partial \tau} + \left(\overline{w_{io,1}^2} + \epsilon'_3 \overline{w_{io,2}^2} + \dots \right) \left(\frac{\partial U_{io,1}}{\partial z_{io}} + \epsilon'_1 \frac{\partial U_{io,2}}{\partial z_{io}} + \epsilon'_1 \epsilon'_3 \frac{\partial U_{io,31}}{\partial z_{io}} + \epsilon'_1 \epsilon'_5 \frac{\partial U_{io,32}}{\partial z_{io}} + \dots \right) \\ & + \epsilon'_1 \left(\left(w \frac{\partial p}{\partial x} \right)_{io,1} + \epsilon'_3 \left(w \frac{\partial p}{\partial x} \right)_{io,2} + \epsilon'_5 \epsilon'_2 \left(w \frac{\partial p}{\partial x} \right)_{io,3} \right) + \dots = 0. \end{aligned} \quad (2.69)$$

$$\begin{aligned} \frac{1}{2} \epsilon'_3 \left(\frac{\partial \overline{w_{io,1}^2}}{\partial \tau} + \epsilon'_3 \frac{\partial \overline{w_{io,2}^2}}{\partial \tau} + \dots \right) &= -\frac{1}{2} \left(\frac{\partial \overline{w_{io,1}^3}}{\partial z_{io}} + \epsilon'_3 \frac{\partial \overline{w_{io,2}^3}}{\partial z_{io}} + \dots \right) + \dots \\ & + \left(\overline{w\theta_{io,1}} + \epsilon'_\theta \overline{w\theta_{io,2}} + \dots \right) - \varepsilon_{3io} \end{aligned} \quad (2.70)$$

$$\begin{aligned} \frac{1}{2} \epsilon'_3 \frac{\partial \overline{u_{io}^2}}{\partial \tau} &= - \left(\overline{uw_{io,1}} + \epsilon'_3 \overline{uw_{io,2}} + \epsilon'_5 \epsilon'_2 \overline{uw_{io,3}} + \dots \right) \left(\frac{\partial U_{io,1}}{\partial z_{io}} + \epsilon'_1 \frac{\partial U_{io,2}}{\partial z_{io}} \right. \\ & + \left. \epsilon'_1 \epsilon'_3 \frac{\partial U_{io,31}}{\partial z_{io}} + \epsilon'_1 \epsilon'_5 \frac{\partial U_{io,32}}{\partial z_{io}} + \dots \right) - \frac{1}{2} \left(\frac{\partial \overline{uw_{io,1}^2}}{\partial z_{io}} + \epsilon'_3 \frac{\partial \overline{uw_{io,21}^2}}{\partial z_{io}} \right. \\ & + \left. \epsilon'_5 \epsilon'_2 \frac{\partial \overline{uw_{io,22}^2}}{\partial z_{io}} + \dots \right) + \dots - \varepsilon_{1io} \end{aligned} \quad (2.71)$$

The time derivative terms are of second order in the inner-outer layer and become of

leading order in the outer layer. Therefore, the leading-order inner-outer solution is not valid for $z \sim z_i$. These terms are a source of the second-order velocity gradient.

2.3. Inner-inner layer

The leading-order inner-outer solution is not valid for $z \sim h_0$, indicating that there is a second inner scaling layer, the roughness layer, which is nested inside the inner-outer layer, which we call the inner-inner layer (Tong & Ding 2020). Therefore, we also need to obtain the inner-inner expansions. We define the non-dimensional inner-inner variables as

$$\begin{aligned} U(z) &= U_m U_{ii} \left(\frac{z}{h_0} \right), \quad V(z) = V_g V_{ii} \left(\frac{z}{h_0} \right), \quad \Theta = \Theta_m \Theta_{ii} \left(\frac{z}{h_0} \right), \quad \overline{uw} = u_*^2 \overline{uw}_{ii}, \quad \overline{vw} = f U_g h_0 \overline{vw}_{ii}, \\ z &= h_0 z_{ii}, \quad \overline{u\theta} = Q \overline{u\theta}_{ii}, \quad t = \frac{z_i}{w_*} \tau, \quad \overline{w^2} = u_*^2 \overline{w^2}_{ii}, \quad \overline{u^2} = u_*^2 \overline{u^2}_{ii}, \quad \overline{w\theta} = Q \overline{w\theta}_{ii}, \quad \overline{\theta^2} = \left(\frac{Q}{u_*} \right)^2 \overline{\theta^2}_{ii}, \\ p &= u_*^2 p_{ii}, \end{aligned} \quad (2.72)$$

Substituting the inner-inner variables given in (2.72) into equations (2.1) to (2.9) we obtain

$$\frac{u_*^2 w_*}{z_i} \frac{\partial \overline{uw}_{ii}}{\partial \tau} + u_*^2 \overline{w^2}_{ii} \frac{U_m}{h_0} \frac{\partial U_{ii}}{\partial z_{ii}} - \frac{g}{T} Q \overline{u\theta}_{ii} + \frac{u_*^3}{h_0} \left(\frac{\partial \overline{uw^2}_{ii}}{\partial z_{ii}} + \left(\overline{w} \frac{\partial p}{\partial x} \right)_{ii} + \left(\overline{u} \frac{\partial p}{\partial z} \right)_{ii} \right) = 0, \quad (2.73)$$

$$f U_g h_0 \frac{w_*}{z_i} \frac{\partial \overline{vw}_{ii}}{\partial \tau} + u_*^2 \overline{w^2}_{ii} \frac{V_g}{h_0} \frac{\partial V_{ii}}{\partial z_{ii}} - \frac{g}{T} Q \overline{v\theta}_{ii} + \frac{u_*}{h_0} f U_g h_0 \left(\frac{\partial \overline{vw^2}_{ii}}{\partial z_{ii}} + \left(\overline{w} \frac{\partial p}{\partial y} \right)_{ii} + \left(\overline{v} \frac{\partial p}{\partial z} \right)_{ii} \right) = 0, \quad (2.74)$$

$$\frac{Q w_*}{z_i} \frac{\partial \overline{w\theta}_{ii}}{\partial \tau} + u_*^2 \overline{w^2}_{ii} \frac{\Theta_m}{h_0} \frac{\partial \Theta_{ii}}{\partial z_{ii}} + \frac{g}{T} \left(\frac{Q}{u_*} \right)^2 \overline{\theta^2}_{ii} + \frac{Q u_*}{h_0} \left(\frac{\partial \overline{w^2\theta}_{ii}}{\partial z_{ii}} + \left(\overline{\theta} \frac{\partial p}{\partial z} \right)_{ii} \right) = 0, \quad (2.75)$$

$$\frac{u_*^2}{h_0} \frac{\partial \overline{uw}_{ii}}{\partial z_{ii}} = f(V - V_g) + \frac{d\tau_{rx}}{dz}, \quad (2.76)$$

$$f U_g \frac{\partial \overline{vw}_{ii}}{\partial z_{ii}} = f(U_g - U) + \frac{d\tau_{ry}}{dz}, \quad (2.77)$$

$$\frac{\Theta_m}{z_i/w_*} \frac{\partial \Theta_{ii}}{\partial \tau} + \frac{Q}{h_0} \frac{\partial \overline{w\theta}_{ii}}{\partial z_{ii}} = 0, \quad (2.78)$$

$$\frac{1}{2} \frac{u_*^2}{z_i/w_*} \frac{\partial \overline{w^2}_{ii}}{\partial \tau} = -\frac{1}{2} \frac{u_*^3}{h_0} \frac{\partial \overline{w^3}_{ii}}{\partial z_{ii}} + \left(\overline{p} \frac{\partial w}{\partial z} \right)_{ii} \frac{u_*^3}{h_0} - \left(\overline{\frac{\partial pw}{\partial z}} \right)_{ii} \frac{u_*^3}{h_0} + \frac{g}{T} Q \overline{w\theta}_{ii} - \varepsilon_3 \quad (2.79)$$

$$\frac{1}{2} \frac{u_*^2}{z_i/w_*} \frac{\partial \overline{u^2}_{ii}}{\partial \tau} = -u_*^2 \overline{uw}_{ii} \frac{u_*}{h_0} \frac{\partial U_{ii}}{\partial z_{ii}} - \frac{1}{2} \frac{u_*^3}{h_0} \frac{\partial \overline{wu^2}_{ii}}{\partial z_{ii}} + \left(\overline{p} \frac{\partial u}{\partial x} \right)_{ii} \frac{u_*^3}{h_0} - \varepsilon_1 \quad (2.80)$$

$$\frac{1}{2} \left(\frac{Q}{u_*} \right)^2 \frac{w_*}{z_i} \frac{\partial \overline{\theta^2}_{ii}}{\partial \tau} = -Q \overline{w\theta}_{ii} \frac{Q}{u_* h_0} \frac{\partial \Theta_{ii}}{\partial z_{ii}} - \frac{1}{2} \left(\frac{Q}{u_*} \right)^2 \frac{u_*}{h_0} \frac{\partial \overline{w\theta^2}_{ii}}{\partial z_{ii}} - \varepsilon_\theta \quad (2.81)$$

Using $u_*^2 U_m/h_0$, Qu_*/h_0 , u_*^2/h_0 , $\Theta_m u_*^2/h_0$, u_*^3/h_0 and $Q^2/u_* h_0$ to non-dimensionalise the shear-stress and vertical flux budgets, as well as to the mean momentum, mean potential temperature and variance equations, leads to the corresponding governing equations for the inner-inner layer

$$\frac{h_0}{z_i} \frac{w_*}{U_m} \frac{\partial \bar{u} \bar{w}_{ii}}{\partial \tau} + \bar{w}_{ii}^2 \frac{\partial U_{ii}}{\partial z_{ii}} - \frac{(g/T) Q h_0}{u_*^2 U_m} \bar{u} \bar{\theta}_{ii} + \epsilon'_1 \left(\frac{\partial \bar{u} \bar{w}^2_{ii}}{\partial z_{ii}} + \left(\bar{w} \frac{\partial \bar{p}}{\partial x} \right)_{ii} + \left(\bar{u} \frac{\partial \bar{p}}{\partial z} \right)_{ii} \right) = 0, \quad (2.82)$$

$$\frac{h_0}{z_i} \frac{f h_0 w_*}{u_*^2} \frac{U_g}{U_m} \frac{\partial \bar{v} \bar{w}_{ii}}{\partial \tau} + \bar{w}_{ii}^2 \frac{V_g}{U_m} \frac{\partial V_{ii}}{\partial z_{ii}} - \frac{(g/T) Q h_0}{u_*^2 U_m} \bar{v} \bar{\theta}_{ii} + \epsilon''_2 \frac{V_g}{U_m} \left(\frac{\partial \bar{v} \bar{w}^2_{ii}}{\partial z_{ii}} + \left(\bar{w} \frac{\partial \bar{p}}{\partial y} \right)_{ii} + \left(\bar{v} \frac{\partial \bar{p}}{\partial z} \right)_{ii} \right) = 0, \quad (2.83)$$

$$\epsilon'_3 \epsilon''_3 \epsilon'_\theta \frac{\partial \bar{w} \bar{\theta}_{ii}}{\partial \tau} + \bar{w}_{ii}^2 \frac{\partial \Theta_{ii}}{\partial z_{ii}} + \epsilon''_3 \epsilon'_\theta \bar{\theta}_{ii}^2 + \epsilon'_\theta \left(\frac{\partial \bar{w}^2 \bar{\theta}_{ii}}{\partial z_{ii}} + \left(\bar{\theta} \frac{\partial \bar{p}}{\partial z} \right)_{ii} \right) = 0, \quad (2.84)$$

$$\frac{\partial \bar{u} \bar{w}_{ii}}{\partial z_{ii}} = \epsilon''_5 - \epsilon''_5 \epsilon''_2 V_{ii,2} + \frac{d \tau_{rxii}}{d z_{ii}} \quad (2.85)$$

$$\frac{\partial \bar{v} \bar{w}_{ii}}{\partial z_{ii}} = 1 - \epsilon''_4 U_{ii,2} + \frac{d \tau_{ryii}}{d z_{ii}} \quad (2.86)$$

$$\epsilon'_3 \epsilon''_3 \frac{\partial \Theta_{ii}}{\partial \tau} + \epsilon'_\theta \frac{\partial \bar{w} \bar{\theta}_{ii}}{\partial z_{ii}} = 0, \quad (2.87)$$

$$\frac{1}{2} \epsilon'_3 \epsilon''_3 \frac{\partial \bar{w}^2_{ii}}{\partial \tau} = -\frac{1}{2} \frac{\partial \bar{w}^3_{ii}}{\partial z_{ii}} + \left(\bar{p} \frac{\partial \bar{w}}{\partial z} \right)_{ii} - \left(\bar{p} \frac{\partial \bar{w}}{\partial z} \right)_{ii} + \epsilon''_3 \bar{w} \bar{\theta}_{ii} - \varepsilon_{3ii} \quad (2.88)$$

$$\frac{1}{2} \epsilon'_3 \epsilon''_3 \frac{\partial \bar{u}^2_{ii}}{\partial \tau} = -\bar{u} \bar{w}_{ii} \frac{\partial U_{ii}}{\partial z_{ii}} - \frac{1}{2} \frac{\partial \bar{w} \bar{u}_{ii}^2}{\partial z_{ii}} + \left(\bar{p} \frac{\partial \bar{u}}{\partial x} \right)_{ii} - \varepsilon_{1ii} \quad (2.89)$$

$$\frac{1}{2} \epsilon'_3 \epsilon''_3 \frac{\partial \bar{\theta}_{ii}^2}{\partial \tau} = -\bar{w} \bar{\theta}_{ii} \frac{\partial \Theta_{ii}}{\partial z_{ii}} - \frac{1}{2} \frac{\partial \bar{w} \bar{\theta}_{ii}^2}{\partial z_{ii}} - \varepsilon_{\theta ii} \quad (2.90)$$

where

$$\epsilon'_1 = \frac{u_*}{U_m}, \quad \epsilon''_2 = \frac{f h_0}{u_*} \frac{U_g}{V_g}, \quad \epsilon''_3 = \frac{h_0}{L}, \quad (2.91)$$

$$\epsilon''_4 = \frac{u_*}{U_g}, \quad \epsilon''_5 = \frac{h_0}{z_i}, \quad \epsilon'_\theta = \frac{Q}{u_* \Theta_m} \quad (2.92)$$

Here ϵ''_2 and ϵ''_4 quantify the effects of the Coriolis force in the U - and V -components of the mean velocity. ϵ''_3 quantifies the effects of the buoyancy production of \bar{w}^2 . ϵ''_5 quantifies the effects of variations of the shear stress with height. ϵ''_θ represents the relative scale of the mean temperature.

The inner-inner expansions are

$$\overline{w_{ii}^2}(z_{ii}) = \overline{w_{ii,1}^2}(z_{ii}) + \epsilon_3'' \overline{w_{ii,2}^2}(z_{ii}) + O(\epsilon_3''), \quad (2.93)$$

$$U_{ii} = U_{ii,1} + \epsilon'_1 U_{ii,2} + \epsilon'_1 \epsilon_3'' U_{ii,31} + \epsilon'_1 \epsilon_5'' U_{ii,32} + \dots \quad (2.94)$$

$$\frac{\partial \overline{uw_{ii}^2}}{\partial z_{ii}} = \frac{\partial \overline{uw_{ii,1}^2}}{\partial z_{ii}} + \epsilon_3'' \frac{\partial \overline{uw_{ii,2}^2}}{\partial z_{ii}} + \epsilon_5'' \epsilon_2'' \frac{\partial \overline{uw_{ii,3}^2}}{\partial z_{ii}} + \dots \quad (2.95)$$

$$V_{ii} = V_{ii,1} + \epsilon_2'' V_{ii,2} + \epsilon_2'' \epsilon_3'' V_{ii,31} + \epsilon_2'' \epsilon_4'' V_{ii,32} + \dots \quad (2.96)$$

$$\frac{\partial \overline{vw_{ii}^2}}{\partial z_{ii}} = \frac{\partial \overline{vw_{ii,1}^2}}{\partial z_{ii}} + \epsilon_3'' \frac{\partial \overline{vw_{ii,21}^2}}{\partial z_{ii}} + \epsilon_4'' \frac{\partial \overline{vw_{ii,22}^2}}{\partial z_{ii}} + \dots \quad (2.97)$$

$$\Theta_{ii} = \Theta_{ii,1} + \epsilon'_\theta \Theta_{ii,2} + \epsilon'_\theta \epsilon_3'' \Theta_{ii,3} + \epsilon'_\theta \epsilon_3' \epsilon_3'' \Theta_{ii,4} + \dots \quad (2.98)$$

Substitute the inner-inner expansions back to equations (2.82), (2.88) and (2.89) we obtain

$$\begin{aligned} & (\overline{w_{ii,1}^2} + \epsilon_3'' \overline{w_{ii,2}^2} + \dots) \left(\frac{\partial U_{ii,1}}{\partial z_{ii}} + \epsilon'_1 \frac{\partial U_{ii,2}}{\partial z_{ii}} + \epsilon'_1 \epsilon_3'' \frac{\partial U_{ii,31}}{\partial z_{ii}} + \epsilon'_1 \epsilon_5'' \frac{\partial U_{ii,32}}{\partial z_{ii}} + \dots \right) \\ & + \epsilon'_1 \left(\left(w \frac{\partial p}{\partial x} \right)_{ii,1} + \epsilon'_3 \left(w \frac{\partial p}{\partial x} \right)_{ii,2} + \epsilon'_5 \epsilon'_2 \left(w \frac{\partial p}{\partial x} \right)_{ii,3} \right) + \dots = 0. \end{aligned} \quad (2.99)$$

$$\begin{aligned} \frac{1}{2} \epsilon'_3 \epsilon_3'' \left(\frac{\partial \overline{w_{ii,1}^2}}{\partial \tau} + \epsilon_3'' \frac{\partial \overline{w_{ii,2}^2}}{\partial \tau} + \dots \right) &= -\frac{1}{2} \left(\frac{\partial \overline{w_{ii,1}^3}}{\partial z_{ii}} + \epsilon_3'' \frac{\partial \overline{w_{ii,2}^3}}{\partial z_{ii}} + \dots \right) \\ & + \dots + \left(\overline{w\theta}_{ii,1} + \epsilon'_\theta \overline{w\theta}_{ii,2} + \dots \right) - \varepsilon_{3ii} \end{aligned} \quad (2.100)$$

$$\begin{aligned} \frac{1}{2} \epsilon'_3 \epsilon_3'' \frac{\partial \overline{u_{ii}^2}}{\partial \tau} &= - \left(\overline{uw}_{ii,1} + \epsilon_3'' \overline{uw}_{ii,2} + \epsilon_5'' \epsilon_2'' \overline{uw}_{ii,3} + \dots \right) \left(\frac{\partial U_{ii,1}}{\partial z_{ii}} + \epsilon'_1 \frac{\partial U_{ii,2}}{\partial z_{ii}} \right. \\ & \left. + \epsilon'_1 \epsilon_3'' \frac{\partial U_{ii,31}}{\partial z_{ii}} + \epsilon'_1 \epsilon_5'' \frac{\partial U_{ii,32}}{\partial z_{ii}} + \dots \right) - \frac{1}{2} \left(\frac{\partial \overline{uw_{ii,1}^2}}{\partial z_{ii}} + \epsilon_3'' \frac{\partial \overline{uw_{ii,21}^2}}{\partial z_{ii}} \right. \\ & \left. + \epsilon_5'' \epsilon_2'' \frac{\partial \overline{uw_{ii,22}^2}}{\partial z_{ii}} + \dots \right) + \dots - \varepsilon_{1ii} \end{aligned} \quad (2.101)$$

The buoyancy production of $\overline{w_{ii,1}^2}$ is of higher order, but becomes leading order in the inner-outer layer. Therefore, it induces the second-order terms in the inner-inner expansions.

2.4. Matching between outer and inner-outer layers

The asymptotic expansions for each layer are valid as long as the location z is away from the other layers. For example, the outer expansions are valid for $-z/L \gg 1$ while inner-outer expansions are valid for $z/z_i \ll 1$ and $z/h_0 \gg 1$. As a result, for $-L \ll z \ll z_i$

both the outer and inner-outer expansions are valid. We can asymptotically match the expansions in this so-called matching or overlapping layer to obtain the scaling of the terms in the expansions. Therefore, asymptotic matching effectively provides additional equations to close the equation set, allowing us to obtain the functional form of the profile in the matching layer, and avoiding the need for a closure model.

We now asymptotically match the third-order outer expansion of the mean velocity with the second-order inner-outer expansion,

$$U = U_m(U_{o,1} + \epsilon_1 U_{o,2} + \epsilon_1 \epsilon_3 U_{o,31} + \epsilon_1 \epsilon_3^2 U_{o,4} + \dots), \quad (2.102)$$

$$U = U_m(U_{io,1} + \epsilon'_1 U_{io,2} + \epsilon'_1 \epsilon'_3 U_{io,31} + \epsilon'_1 \epsilon'_5 U_{io,32} + \dots). \quad (2.103)$$

Here we include the $\epsilon'_1 \epsilon'_5$ term which is smaller than $\epsilon'_1 \epsilon'_3$, but is larger than the next-order term $\epsilon'_1 \epsilon'_3^2$. In general, matching is performed by taking intermediate limits $\epsilon_i \rightarrow 0$ and $z_o \rightarrow 0$ for the outer expansions and $\epsilon'_i \rightarrow 0$ and $z_{io} \rightarrow \infty$ for the inner-outer expansions (Bender & Orszag 1978). However, matching between the terms of the same order alone is often insufficient. According to van Dyke's matching principle (van Dyke 1975), the same number of terms in the inner expansion of the outer expansion and the outer expansion of the inner expansion need to be matched. Therefore, matching across the orders is generally necessary.

Matching the expansions of the same orders results in

$$U_{o,1} = U_{io,1}, \quad \epsilon_1 U_{o,2} = \epsilon'_1 U_{io,2} \dagger, \quad \epsilon_1 \epsilon_3 U_{o,31} = \epsilon'_5 \epsilon'_1 U_{io,32}, \quad \epsilon_1 \epsilon_3 U_{o,31} = \epsilon'_1 \epsilon'_3 U_{io,31}, \quad (2.104)$$

leading to

$$U_{o,1} = U_{io,1} = 1, \quad (2.105)$$

$$U_{o,21} = A\left(\frac{z}{z_i}\right)^{-1/3}, \quad U_{io,21} = A\left(-\frac{z}{L}\right)^{-1/3}, \quad (2.106)$$

$$U_{o,311} = B\left(\frac{z}{z_i}\right)^{-2/3}, \quad U_{io,321} = B\left(-\frac{z}{L}\right)^{-2/3}, \quad (2.107)$$

$$U_{o,312} = J\left(\frac{z}{z_i}\right)^{-1}, \quad U_{io,311} = J\left(-\frac{z}{L}\right)^{-1}. \quad (2.108)$$

[†] Strictly speaking, this equation should be $\lim_{\epsilon_1, z_o \rightarrow 0} \epsilon_1 U_{o,2} = \lim_{\epsilon'_1 \rightarrow 0, z_{io} \rightarrow \infty} \epsilon'_1 U_{io,2}$. To simplify the notations, we omit the limits. The other equations are written in a similar manner.

Matching the expansions of different orders (cross-order matching) gives

$$\epsilon_1 U_{o,2} = \epsilon'_1 \epsilon'_3 U_{io,31}, \quad \epsilon_1 \epsilon_3 U_{o,31} = \epsilon'_1 U_{io,2}, \quad \epsilon_1 U_{o,2} = \epsilon'_1 \epsilon'_5 U_{io,32}. \quad (2.109)$$

$$\epsilon_1 \epsilon_3^2 U_{o,41} = \epsilon'_1 U_{io,2}, \quad \epsilon_1 \epsilon_3^2 U_{o,42} = \epsilon'_1 \epsilon'_5 U_{io,32}, \quad \epsilon_1 \epsilon_3^2 U_{o,43} = \epsilon'_1 \epsilon'_3 U_{io,31}, \quad (2.110)$$

The results of the matching process (details given in Appendix A) are

$$U_{o,22} = D\left(\frac{z}{z_i}\right)^{1/3}, \quad U_{io,312} = D\left(-\frac{z}{L}\right)^{1/3}, \quad (2.111)$$

$$U_{o,313} = E\left(\frac{z}{z_i}\right)^{-5/3}, \quad U_{io,22} = E\left(-\frac{z}{L}\right)^{-5/3}, \quad (2.112)$$

$$U_{o,23} = F\left(\frac{z}{z_i}\right)^{2/3}, \quad U_{io,322} = F\left(-\frac{z}{L}\right)^{2/3}, \quad (2.113)$$

$$U_{o,41} = G\left(\frac{z}{z_i}\right)^{-3}, \quad U_{io,23} = G\left(-\frac{z}{L}\right)^{-3}, \quad (2.114)$$

$$U_{o,42} = H\left(\frac{z}{z_i}\right)^{-2}, \quad U_{io,323} = H\left(-\frac{z}{L}\right)^{-2}, \quad (2.115)$$

$$U_{o,43} = I\left(\frac{z}{z_i}\right)^{-7/3}, \quad U_{io,313} = I\left(-\frac{z}{L}\right)^{-7/3}, \quad (2.116)$$

Inserting the matching results into equations (2.30) and (2.62), we obtain the higher-order asymptotic expansions for the local-free-convection layer in terms of the outer and inner-outer variables respectively

$$\begin{aligned} U_o &= U_{o,1} + \epsilon_1 U_{o,21} + \epsilon_1 U_{o,22} + \epsilon_1 U_{o,23} + \epsilon_1 \epsilon_3 U_{o,311} + \epsilon_1 \epsilon_3 U_{o,312} + \epsilon_1 \epsilon_3 U_{o,313} \\ &\quad + \epsilon_1 \epsilon_3^2 U_{o,41} + \epsilon_1 \epsilon_3^2 U_{o,42} + \epsilon_1 \epsilon_3^2 U_{o,43} + \dots \\ &= 1 + \epsilon_1 A\left(\frac{z}{z_i}\right)^{-1/3} + \epsilon_1 D\left(\frac{z}{z_i}\right)^{1/3} + \epsilon_1 F\left(\frac{z}{z_i}\right)^{2/3} + \epsilon_1 \epsilon_3 B\left(\frac{z}{z_i}\right)^{-2/3} + \epsilon_1 \epsilon_3 J\left(\frac{z}{z_i}\right)^{-1} \\ &\quad + \epsilon_1 \epsilon_3 E\left(\frac{z}{z_i}\right)^{-5/3} + \epsilon_1 \epsilon_3^2 G\left(\frac{z}{z_i}\right)^{-3} + \epsilon_1 \epsilon_3^2 H\left(\frac{z}{z_i}\right)^{-2} + \epsilon_1 \epsilon_3^2 I\left(\frac{z}{z_i}\right)^{-7/3} + \dots \end{aligned} \quad (2.117)$$

$$\begin{aligned} U_{io} &= U_{io,1} + \epsilon'_1 U_{io,21} + \epsilon'_1 U_{io,22} + \epsilon'_1 U_{io,23} + \epsilon'_1 \epsilon'_3 U_{io,311} + \epsilon'_1 \epsilon'_3 U_{io,312} + \epsilon'_1 \epsilon'_3 U_{io,313} \\ &\quad + \epsilon'_5 \epsilon'_1 U_{io,321} + \epsilon'_5 \epsilon'_1 U_{io,322} + \epsilon'_5 \epsilon'_1 U_{io,323} + \dots \\ &= 1 + \epsilon'_1 A\left(-\frac{z}{L}\right)^{-1/3} + \epsilon'_1 E\left(-\frac{z}{L}\right)^{-5/3} + \epsilon'_1 G\left(-\frac{z}{L}\right)^{-3} + \epsilon'_1 \epsilon'_3 J\left(-\frac{z}{L}\right)^{-1} + \epsilon'_1 \epsilon'_3 D\left(-\frac{z}{L}\right)^{1/3} \\ &\quad + \epsilon'_1 \epsilon'_3 I\left(-\frac{z}{L}\right)^{-7/3} + \epsilon'_5 \epsilon'_1 B\left(-\frac{z}{L}\right)^{-2/3} + \epsilon'_5 \epsilon'_1 F\left(-\frac{z}{L}\right)^{2/3} + \epsilon'_5 \epsilon'_1 H\left(-\frac{z}{L}\right)^{-2} + \dots \end{aligned} \quad (2.118)$$

2.5. Matching between inner-outer and inner-inner layer

Matching mean velocity between the inner-outer and inner-inner layer is performed by taking the intermediate limits $\epsilon'_i \rightarrow 0$ and $z_{io} \rightarrow 0$ for the inner-outer expansions, and

$\epsilon'_i \rightarrow 0$ and $z_{ii} \rightarrow \infty$ for the inner-outer expansions. The expansions are

$$U_{io} = U_{io,1} + \epsilon'_1 U_{io,2} + \dots \quad (2.119)$$

$$U_{ii} = U_{ii,1} + \epsilon'_1 U_{ii,2} + \epsilon'_1 \epsilon''_3 U_{ii,32} + \epsilon'_1 \epsilon''^2_3 U_{ii,41} + \dots \quad (2.120)$$

Matching the expansion terms of the same order results in the log law

$$U_{io,1} + \epsilon'_1 U_{io,2} = \epsilon'_1 U_{ii,2}, \quad (2.121)$$

$$U_{io,21} = A' \frac{1}{\kappa} \ln(-\frac{z}{L}) + C, \quad U_{ii,2} = A' \frac{1}{\kappa} \ln(\frac{z}{h_0}), \quad (2.122)$$

Cross-order matching (details are in Appendix A) gives

$$\epsilon'_1 U_{io,2} = \epsilon'_1 \epsilon''_3 U_{ii,32}, \quad \epsilon'_1 U_{io,2} = \epsilon'_1 \epsilon''^2_3 U_{ii,41}, \quad (2.123)$$

$$U_{io,22} = C'(-\frac{z}{L}), \quad U_{ii,32} = C' \frac{z}{h_0}, \quad (2.124)$$

$$U_{io,23} = E'(-\frac{z}{L})^2, \quad U_{ii,41} = E'(\frac{z}{h_0})^2, \quad (2.125)$$

The matching results in terms of the inner-outer and inner variables are

$$\begin{aligned} U_{io} &= U_{io,1} + \epsilon'_1 U_{io,21} + \epsilon'_1 U_{io,22} + \epsilon'_1 U_{io,23} + \dots \\ &= 1 + \epsilon'_1 A' \frac{1}{\kappa} \ln(-\frac{z}{L}) + \epsilon'_1 C + \epsilon'_1 C'(-\frac{z}{L}) + \epsilon'_1 E'(-\frac{z}{L})^2 + \dots, \end{aligned} \quad (2.126)$$

$$\begin{aligned} U_{ii} &= U_{ii,1} + \epsilon'_1 U_{ii,2} + \epsilon'_1 \epsilon''_3 U_{ii,32} + \epsilon'_1 \epsilon''^2_3 U_{ii,41} + \dots \\ &= \epsilon'_1 A' \frac{1}{\kappa} \ln(\frac{z}{h_0}) + \epsilon'_1 \epsilon''_3 C' \frac{z}{h_0} + \epsilon'_1 \epsilon''^2_3 E'(\frac{z}{h_0})^2 + \dots, \end{aligned} \quad (2.127)$$

Equating the RHS of equations (2.126) and (2.127) the convective logarithmic friction law is obtained

$$\frac{U_m}{u_*} + C = \frac{1}{\kappa} \ln(-\frac{L}{h_0}), \quad (2.128)$$

This friction law, while identical to the leading-order friction law derived by Tong & Ding (2020), is valid up to the second order (likely is valid to all orders as we do not foresee any higher-order logarithmic expansion terms). Therefore, there are no other parameters in the friction law. This situation is in contrast to channel and pipe flows with smooth walls, where the logarithmic frictional law is a leading-order approximation (Tennekes 1968; Afzal 1976).

3. Determination of expansion coefficients using field data

3.1. Field data

The asymptotic expansions provide the functional forms of the higher-order profile in the matching layers. However, they contain non-dimensional universal expansion coefficients, which need to be determined using field measurement data. To obtain the coefficients and to validate the expansions, a field campaign code-named Multi-point Monin–Obukhov Similarity Horizontal Array Turbulence Study (M²HATS) was conducted from July to September 2023 in Tonopah, Nevada, the United States. A comprehensive suite of in situ and remote sensing instruments was deployed to characterize the convective boundary layer under approximately horizontally homogeneous conditions (Tong *et al.* 2026). The dataset used for obtaining the mean profiles includes quality-controlled surface meteorology and flux measurements from towers including 3D sonic anemometers, and data from a Doppler lidar system (WindCube 200S). The anemometer were mounted at multiple heights (0.62, 1.17, 2.11, 3.02, 4.20, 6.89, 15.45, 28.55 m) and had a native sampling rate of 60 samples/s. The lidar performed continuous plan–position indicator (PPI) scans at a 35.3° elevation angle, with a azimuth coverage from 2° to 360°, an angular resolution of 2.5°, and a typical scan rate of 1 revolution per minute. These measurements provide coverage from 0.62 m to over 3 km above ground level, ensuring accurate determination of stability parameters and mixed-layer variables such as u_* , L , and z_i . This dataset covers a range of z_i/L and h_0/L values, enabling validation of the leading-order velocity profile in the surface layer (the log-law and the local-free-convection scaling) as well as determination of the non-dimensional coefficients in the higher-order asymptotic expansions that account for finite scale separations (z_i/L and h_0/L), thereby providing improved characterization of the mean velocity profile in the CBL.

During the field campaign, daily catalogs (07:00–21:00 local time) were compiled, including: vertical lidar w -wind profiles, sky photographs every two hours, virtual potential temperature and mixing ratio profiles from sondes, potential temperature, humidity, and backscatter measurements from MicroPulse Differential Absorption Lidar (MPD), 10-minute statistics from sonic anemometers, raw u , v , w , T signals from the sonic anemome-

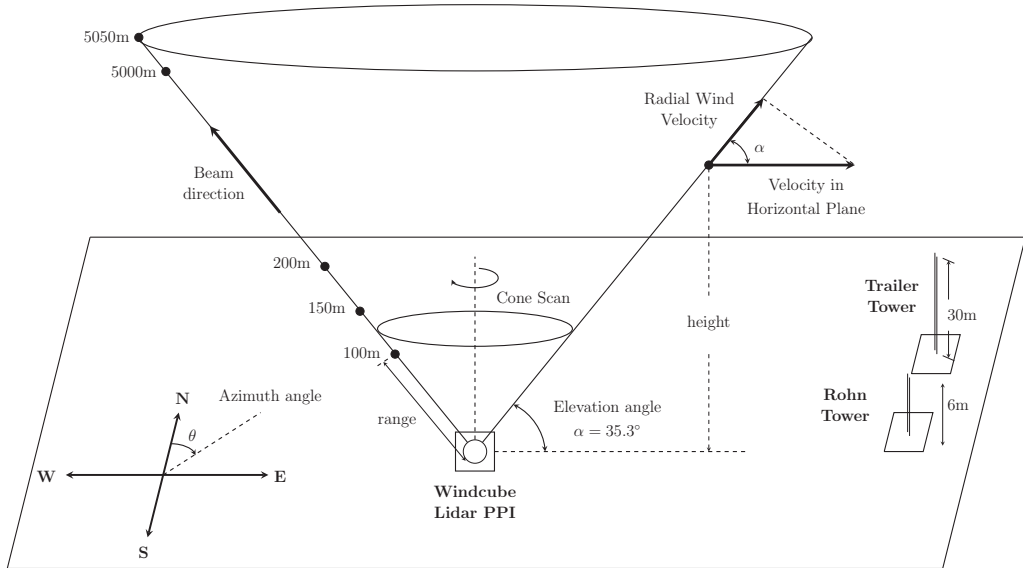


Figure 1: Schematic of the measurement set-up for obtaining the mean profile. Two met towers, 6 m and 32 m in height respectively, provided the mean velocity, the mean shear stress, flux, and gradients near the surface. A Doppler lidar performing Plan Position Indicator (PPI or cone) scan, was used to measure the mean horizontal velocity profiles throughout the boundary layer.

ters. From these data, 91 stationary periods were manually selected for the flux towers. The boundary-layer height z_i was determined using the MPD, lidar, and sonde measurements. Among the periods, 14 were selected for the barotropic cases (Tong *et al.* 2026)

3.2. Procedure for the local-free-convection layer

The data analysis for the local-free-convection layer is conducted using a multi-step procedure to accurately characterising the mean velocity profile and to obtain the expansion coefficients. The procedure includes (i) selecting suitable periods and extracting velocity data from the Doppler lidar signals, (ii) identifying the suitable height range for the leading-order scaling, (iii) iteratively estimating the expansion coefficients using a combination of linear regression, (iv) stabilizing the coefficients using ridge regression (Hoerl & Kennard 1970), and (v) quantifying the uncertainties of the coefficients via bootstrap resampling. The following sections describe each of these steps in detail.

3.2.1. Determination of leading-order matching region

To identify the height range in which the leading-order scaling of the mean velocity (defect) profile, $(z/L)^{-1/3}$, is approximately valid, we perform a systematic search for the lower (in terms of $-z/L$) and upper (in terms of z/z_i) bounds of each profile. To directly identify the height range in which the leading-order scaling of the mean velocity (defect) profile, $(z/L)^{-1/3}$, is approximately valid, one needs the mixed-layer velocity scale U_m , which is not available at this point of the data analysis. To circumvent the need for U_m , for each profile we average the velocity defect over the scaling layer

$$\left(\frac{\overline{U}}{u_*} - \frac{U_m}{u_*} \right) = a \overline{(z/L)^{-1/3}}, \quad (3.1)$$

where the coefficient a has the same value for all the profiles. Subtracting this equation from the velocity defect law, we have

$$\left(\frac{\overline{U}}{u_*} - \frac{U}{u_*} \right) = a \left[\overline{(z/L)^{-1/3}} - (z/L)^{-1/3} \right]. \quad (3.2)$$

If the data approximately satisfies equation (3.2), a height range for the $(z/L)^{-1/3}$ scaling has been identified without using U_m/u_* . Since a is the same for all the profiles which have different U_m/u_* values, we can combine all the data to evaluate the accuracy of the linear relationship. We then perform a least-squares linear regression, and use the coefficient of determination (R^2) to quantify the goodness of fit.

Starting from the range $z = -L$ to $z = 0.2z_i$ and progressively reducing it, the optimal height range is identified as the one yielding the maximum R^2 , i.e., the range where the data most closely follow the theoretical leading-order scaling. In figure 2, the selected interval for matching layer of outer and inner-outer layers has shown.

3.2.2. Iterative procedure for determining expansion coefficients

Here we briefly describe the procedure and provide the details in Appendix B. The non-dimensional velocity profile is expressed as an asymptotic expansion in the powers of $(-z/L)$, including one leading-order term and three higher-order terms. The resulting expression used for the parameter estimation is

$$\frac{U}{u_*} = \frac{U_m}{u_*} + A \left(-\frac{z}{L} \right)^{-1/3} + E \left(-\frac{z}{L} \right)^{-5/3} + G \left(-\frac{z}{L} \right)^{-3} + \epsilon'_3 D \left(-\frac{z}{L} \right)^{1/3}, \quad (3.3)$$

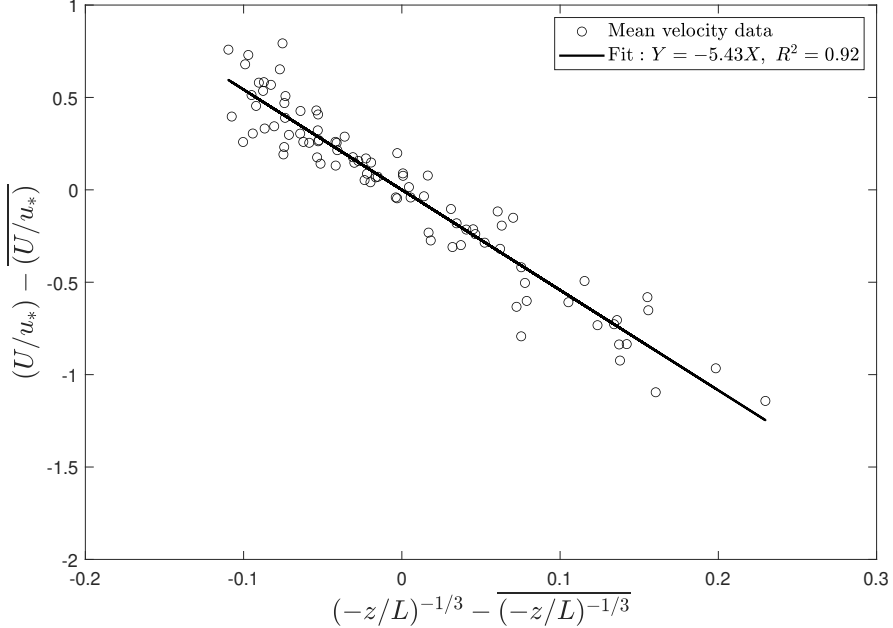


Figure 2: Selected non-dimensional height range for matching between the outer and inner-outer layers

The coefficients A , E , D , G , and the U_m/u_* values are determined using an iterative multi-step procedure which is explained in Appendix B. We do not include the terms containing the coefficients F , H , I and J (equations (2.117) and (2.118)) in the regression due to the size of the data. To stabilize the regression coefficients and prevent unrealistically large values of the higher-order coefficients, we employ ridge regression as a regularization strategy (Willoughby 1979). The mathematical formulation of the ridge-regularized regression and implementation details are provided in Appendix C. To assess the statistical uncertainty of the fitted coefficients, we apply a bootstrap resampling approach, which enables estimation of coefficient variability without assuming any particular error distribution. The bootstrap methodology and its implementation in the present analysis are described in Appendix D.

3.3. Procedure for the log layer

In the surface layer, for $z > -0.1L$ the deviations of measurement data from the logarithmic form is clearly visible. As a result, direct identification of the log layer and the determination of the von Kármán constant is nearly impossible. However, the results

obtained from matching of the inner-outer and inner-inner layers show that, by including the first and second higher-order terms, we can still obtain the coefficients in the higher-order expansions as well as the von Kármán constant from the measurements.

The expansions in terms of the inner-outer and inner-inner variables are

$$U_{io} = 1 + \epsilon'_1 \frac{1}{\kappa} \ln(-\frac{z}{L}) + \epsilon'_1 C'(-\frac{z}{L}) + \epsilon'_1 C' \alpha(-\frac{z}{L})^2 + \epsilon'_1 C, \quad (3.4)$$

$$U_{ii} = \epsilon'_1 \frac{1}{\kappa} \ln(\frac{z}{h_0}) + \epsilon'_1 \epsilon''_3 C' \frac{z}{h_0} + \epsilon'_1 \epsilon''_3 C' \alpha(\frac{z}{h_0})^2, \quad (3.5)$$

The second equation can be written as

$$\frac{U}{u_*} = \frac{1}{\kappa} \ln\left(\frac{z}{h_0}\right) + C' \left(\epsilon''_3 \frac{z}{h_0} + \alpha (\epsilon''_3)^2 \left(\frac{z}{h_0}\right)^2 \right), \quad \epsilon''_3 = \frac{h_0}{-L} \quad (3.6)$$

which can be further written as

$$\frac{U}{u_*} = \frac{1}{\kappa} \ln(z) - \frac{1}{\kappa} \ln(h_0) + C'(-\frac{z}{L}) + C' \alpha(-\frac{z}{L})^2, \quad (3.7)$$

where $C' \alpha = E'$ is a higher-order expansion coefficient. To determine the expansion coefficients, a linear regression is performed to fit the equation

$$Y = \frac{1}{\kappa} X_1 - \frac{1}{\kappa} \ln(h_0) + C' X_2 + C' \alpha X_3, \quad (3.8)$$

where

$$Y = \frac{U}{u_*}, \quad X_1 = \ln(z), \quad X_2 = (-\frac{z}{L}), \quad X_3 = (-\frac{z}{L})^2, \quad (3.9)$$

The term $-\frac{1}{\kappa} \ln(h_0)$ is the intercept and determines the roughness height. In this analysis, the regression procedure is applied to the flux tower data. Specifically, data points are considered for heights ranging from $z = 1$ m up to $z = 1.3|L|$. We find that the higher-order asymptotic expansions agree well with the data within this height range. To quantify the statistical uncertainty associated with the estimated expansion coefficients (κ , C' , $C' \alpha$, and h_0), we again employ the bootstrap resampling approach described in Appendix D.

4. Expansion coefficients and validation of prediction

In this section we will discuss the higher-order expansion coefficients obtained from matching the outer and inner-outer layers, and from matching the inner-outer and inner-

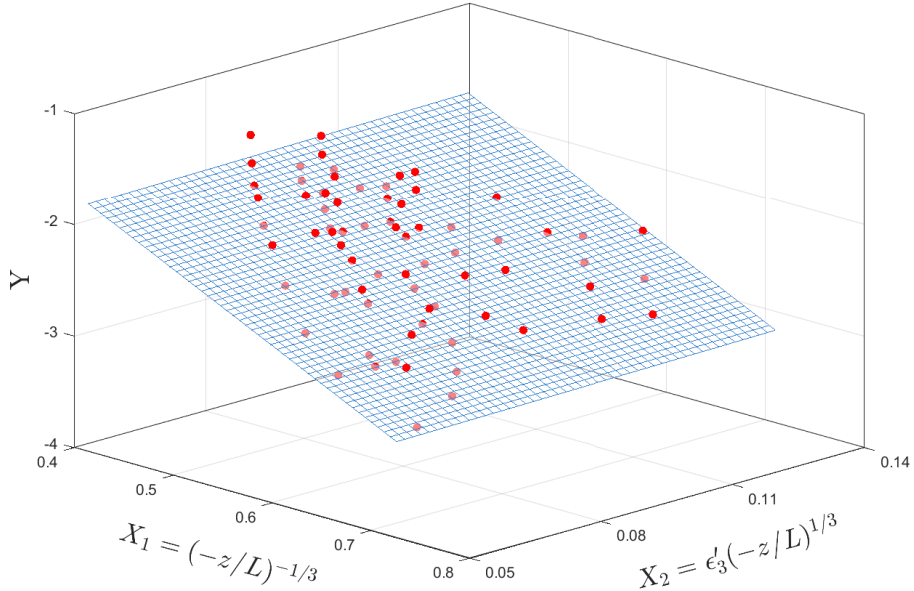


Figure 3: Planar fit of the expansion coefficients to data in the matching region between the outer and inner-outer layers (local-free-convection layer). The variable, $Y = \frac{U}{u_*} - \frac{U_m}{u_*} - E(-\frac{z}{L})^{-5/3} - G(-\frac{z}{L})^{-3}$, is plotted on the vertical axis. The slopes of the planar fit yield the coefficients A and D associated with the $X_1 = (-\frac{z}{L})^{-1/3}$ and $X_2 = \epsilon_3'(-\frac{z}{L})^{1/3}$ terms, respectively. Darker and lighter symbols are above and below the plane respectively.

inner layers. These coefficients have been obtained based on the methods discussed in the previous section. The resulting asymptotic expansions are validated with the data.

4.1. Local-free-convection layer

As discussed in §3.2.2, the expansion coefficients that result from matching between the outer and inner-outer layers are determined using an iterative regression procedure. To stabilise the estimation and mitigate the effects of multicollinearity, ridge regression (Hoerl & Kennard 1970) is employed, with the regularisation parameter λ varied over the range $10^{-5} \leq \lambda \leq 1$. The optimal value of λ is selected using the corner criterion, yielding $\lambda = 0.0196$. The resulting expansion coefficients are

$$A = -4.37, \quad E = -1.58, \quad D = 0.57, \quad G = -0.23.$$

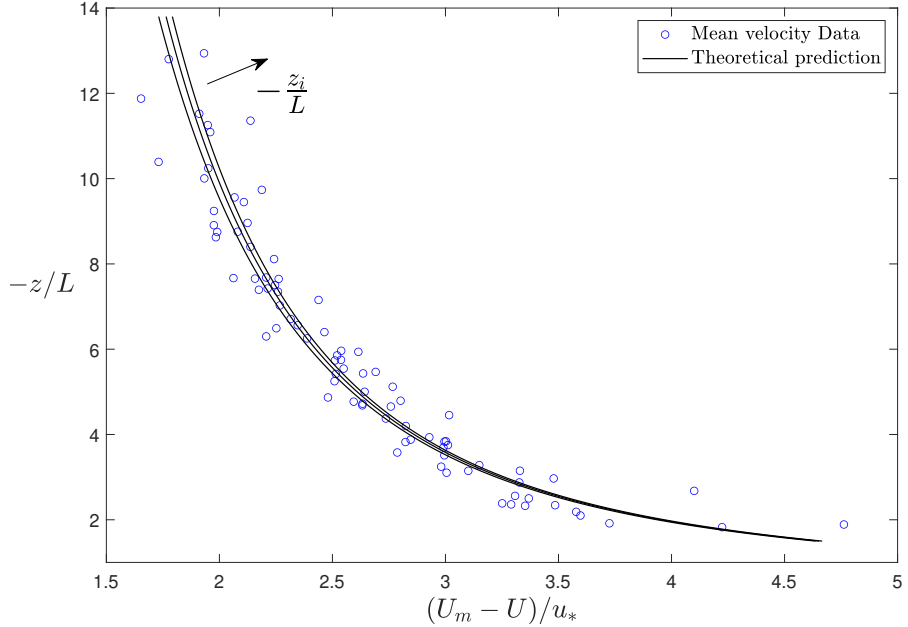


Figure 4: Mean velocity profiles (velocity defect) in the local-free-convection layer. The measured data are shown as circles, and the black curves denote the predicted mean velocity profiles for a range of stability conditions characterized by different values of $-z_i/L$: 43.6, 74.3 and 146.2.

Figure 3 shows the velocity defect minus the (higher-order) contributions from the terms containing E and G , denoted by the symbol Y , plotted as a function of the leading-order variable $X_1 = (-z/L)^{-1/3}$ and the second-order variable $X_2 = \epsilon'_3(-z/L)^{1/3}$. The figure also illustrates the planar fitting procedure used in the regression. The remaining defect Y depends linearly on the leading-order contribution proportional to A and on the higher-order term proportional to D . Therefore the dependence can be represented as a plane. The plane fits the data points well with little scatter, demonstrating the validity of the asymptotic expansions and the regression procedure.

The predicted velocity profiles in the local free-convection layer are presented for several stationary periods in figure 4. The measured mean velocity is shown as circles in terms of the non-dimensional velocity defect $(U_m - U)/u_*$, plotted against the dimensionless height $-z/L$. The predicted profiles, shown as solid black lines, are obtained from the asymptotic representation using the expansion coefficients determined from the

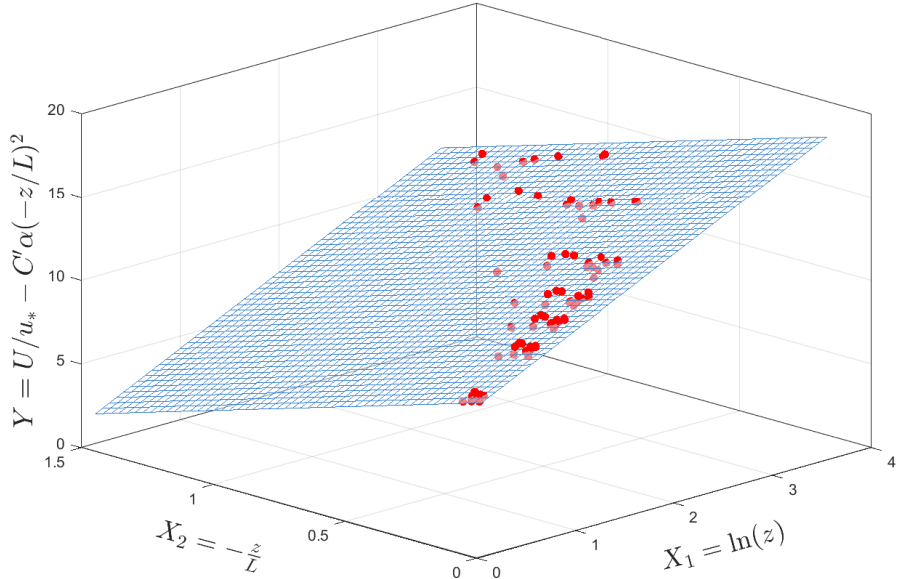


Figure 5: Planar fit of the velocity-profile in the log-law layer. The fit yields the inverse of the von Kármán constant and the coefficient of the first higher-order term, which accounts for a part of the deviations from the logarithmic velocity profile. Symbols same as in figure 3.

matching procedure.

$$\frac{U - U_m}{u_*} = A(-z/L)^{-1/3} + E(-z/L)^{-5/3} + \epsilon'_3 D(-z/L)^{1/3} + G(-z/L)^{-3}, \quad (4.1)$$

The leading-order term dominates the velocity defect over most of the local-free-convection layer and determines the overall profiles. The higher-order term containing E (asymptotically small for $-z/L \gg 1$), together with that containing G (the next higher-order term), acts predominantly at lower heights in the inner-outer matching region, where departures from pure leading-order behaviour become significant.

The term with the coefficient D contains the small perturbation parameter ϵ'_3 ; therefore its contribution is of higher-order for $-z/L \sim 1$, but increases with height. It is responsible for the separation at large $-z/L$ of the predicted profiles for different z_i/L values, which are valid in the overlapping layer between the outer and inner-outer layers. The close overall agreement between the asymptotic expansions and the observations for

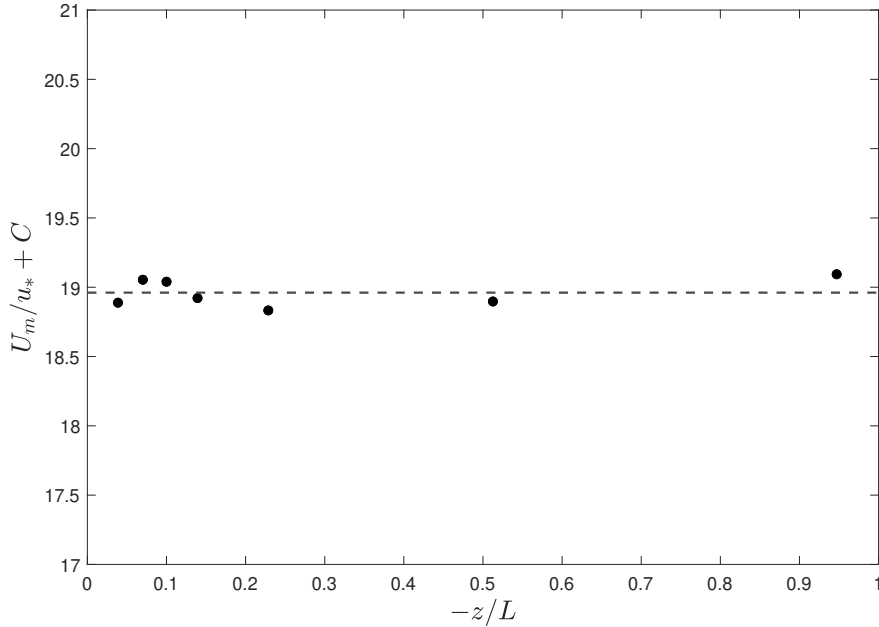


Figure 6: Non-dimensional mixed-layer mean velocity scale U_m evaluated using data at different heights during the period 11:20–15:16 PDT on 26 August 2023.

all the stationary periods considered validates the prediction of the asymptotic analysis and confirms the robustness of the regression procedure.

Given the relatively large statistical uncertainties associated with the mean velocity profiles, it would not be possible to accurately obtain the expansion coefficients if the expansion is used to fit individual profiles. However, when the set of all the suitable profiles are used, the data size increases significantly, thereby resulting in a more accurate regression. Similarly, comparisons of the asymptotic expansions to the measured mean velocity should also be made by comparing the expansions to a set of profiles with different parameters, not to the individual profiles.

4.2. Log law layer

To determine the coefficients in the matching layer between the inner-outer and inner-inner layers, flux tower measurements of the mean velocity are used. The regression is also carried out by representing the equation in the form of a plane. Data points are considered for heights ranging from $z = 1$ m up to $z = 1.3|L|$. We find that within this

range we are able to identify the leading-order (the log law) and the higher-order terms. Figure 5 illustrates the fitted plane obtained from the regression analysis.

The regression procedure yields the following coefficient values for the surface-layer formulation. The value of the von Kármán constant, the stability correction parameters, and the roughness height are obtained

$$\kappa = 0.344, \quad C' = -4.841, \quad C'\alpha = 1.861, \quad h_0 = 0.045 \text{ m.} \quad (4.2)$$

Again, given the uncertainties in the individual profiles, determination of the expansion coefficients with good accuracy is only possible using the set of all the suitable profiles. The roughness length obtained falls within the range commonly reported for unstable atmospheric surface layer with similar terrain. The von Kármán constant is close that obtained by Businger *et al.* (1971), but is smaller than the values obtained in many field measurements (Högström 1996). However, the previous values were invariably obtained by fitting the log law, the leading-order profile, to the measured profile, which includes contributions from the higher-order terms. Since the coefficient for the second-order term, C' , is negative (equation (4.2)), these values tend to underestimate the leading-order term, and therefore overestimate κ . It would be useful to apply our procedure to a wider range of data to further investigate the issue of the value of the von Kármán constant.

The matching results between the inner-inner and inner-outer layers can also be represented as the surface-layer velocity defect

$$\frac{U - U_m}{u_*} = \frac{1}{\kappa} \ln\left(-\frac{z}{L}\right) + C + C' \left[\left(-\frac{z}{L}\right) + \alpha \left(-\frac{z}{L}\right)^2 \right], \quad (4.3)$$

The expression can be rearranged as

$$\frac{U_m}{u_*} + C = \frac{U}{u_*} - \left[\frac{1}{\kappa} \ln\left(-\frac{z}{L}\right) + C' \left(\left(-\frac{z}{L}\right) + \alpha \left(-\frac{z}{L}\right)^2 \right) \right]. \quad (4.4)$$

Here, the quantity $\frac{U_m}{u_*} + C$ represents an offset arising from the matching condition between the inner-outer and inner-inner layers. For each velocity profile, the right-hand side of the equation can be evaluated at all available heights, yielding multiple estimates of this offset. An example for a single stationary period is shown in figure 6, where the evaluated values of $\frac{U_m}{u_*} + C$ are plotted as a function of height. The values obtained

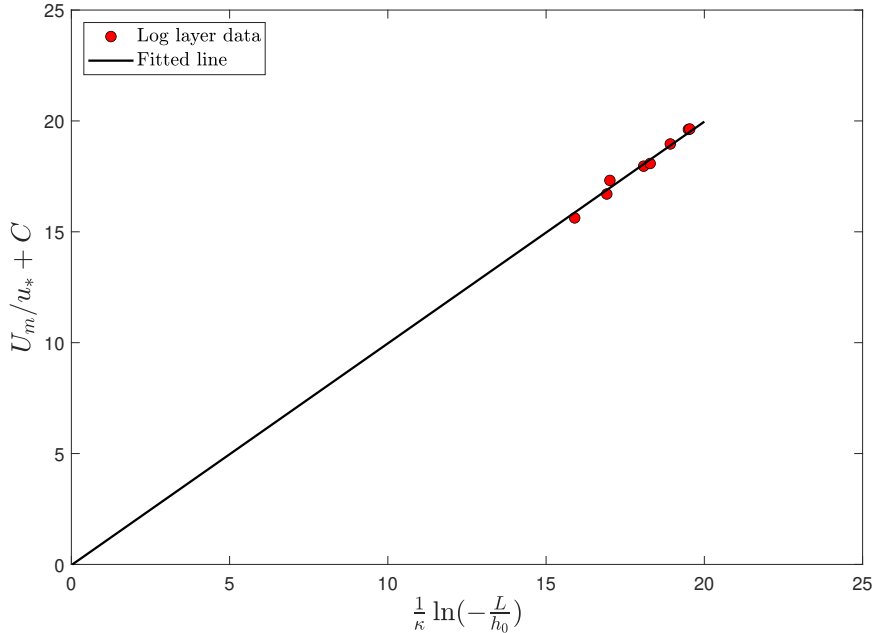


Figure 7: Comparison between the convective logarithmic friction law and data obtained in the log-law layer. The constant C is combined with U_m/u_* . The line represents the friction law.

at different heights show minimal variations, indicating that the procedure provides an accurate estimate of the offset. The average of these values is therefore taken as the estimate of $\frac{U_m}{u_*} + C$ for that profile. This procedure provides an effective way to evaluate the constant C .

The offset, which contains the non-dimensional mixed-layer mean velocity scale, U_m/u_* , can be used to validate the convective logarithmic friction law. In figure 7, the values of $U_m/u_* + C$ are plotted against $\frac{1}{\kappa} \ln(-L/h_0)$. The unity slope of the linear fit indicates the validity of the friction law. The fact that different data points have different z_i/L values confirms that the validity of the friction law extends beyond the leading order.

Using the values of $U_m/u_* + C$ obtained from matching the inner-outer and inner-inner layers for each profile, and the values of U_m/u_* (section 4.1), the constant is determined to be $C = -2.13$. The U_m/u_* values obtained from both the local free-convection layer and the log-law layer can also be used to validate the friction law (figure 8). The results

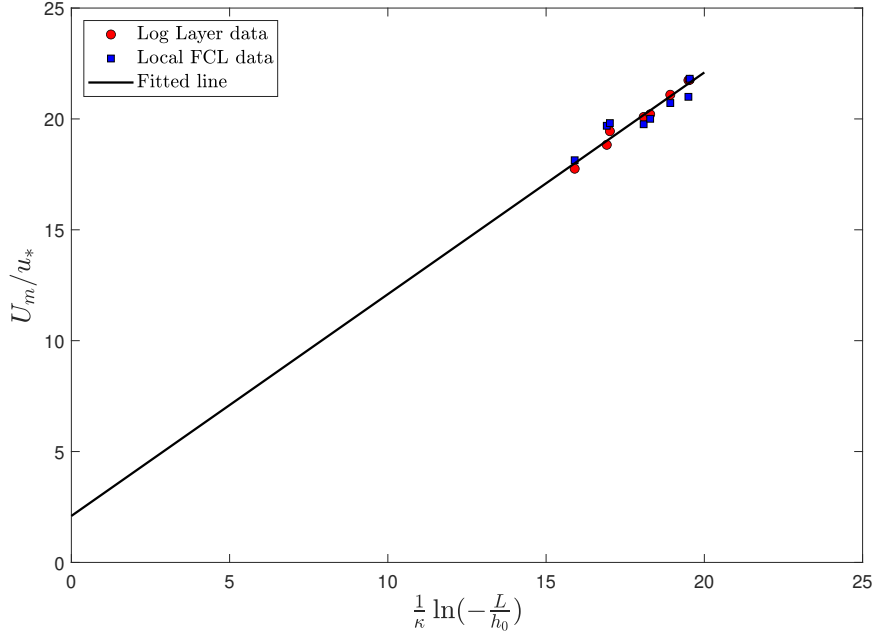


Figure 8: Comparison between the convective friction law and U_m/u_* obtained using data in both matching layers. Circles and squares denote results from the log-law layer and the local-free-convection layer respectively. The line represents the friction law.

from both matching layers are nearly identical, demonstrating that the efficacy of the data analysis procedure.

The mean velocity profile near the surface, U/u_* , is plotted against the non-dimensional height z/h_0 in figure 9. Very close to the surface, all curves nearly collapse, indicating the dominance of the logarithmic term. As the height increases, the curves begin to separate due to the influence of higher-order corrections associated with the small non-dimensional parameter $\epsilon_3'' = -\frac{h_0}{L}$, which accounts for the effects of the buoyancy production. Although ϵ_3'' is small, its contribution becomes increasingly noticeable at larger z/h_0 , allowing the expansions to better approximate the measured velocity profile up to $-z/L \sim 1$. We note that for the data set used, $-z/L$ is generally larger than 0.1. As a result, one can hardly identify a logarithmic profile, let alone determining the von Kármán constant. However, fitting the higher-order asymptotic expansion to the set of data as a whole allows us to accurately identify the log term, the von Kármán constant and the higher-order expansion coefficients.

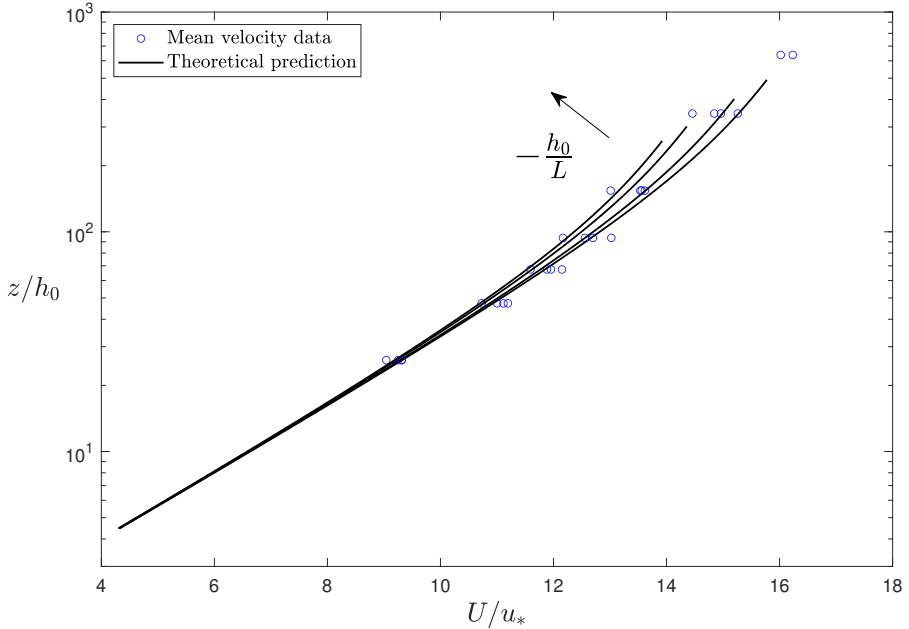


Figure 9: Mean velocity profiles in the matching layer between the Inner–outer and Inner–inner layers (Log–law layer). The measured data are plotted as blue circles, and the black curves denote the predicted mean velocity profiles for a range of stability conditions characterized by different values of $-\frac{h_0}{L}$: $(1.23, 1.49, 1.99, 2.31) \times 10^{-3}$

5. Conclusions

We derived the higher-order mean velocity profile in the convective atmospheric boundary layer (CBL) using the method of matched asymptotic expansions and obtained the expansion coefficients using the measurement data from the recent M²HATS field campaign.

Tong & Ding (2020) have identified the three scaling layers, the mixed or outer layer, the Monin-Obukhov or inner-outer layer and the roughness or inner-inner layer. In this work, for each layer a set of non-dimensional perturbation equations containing small (non-MOST) parameters was obtained using the Reynolds-stress, potential-temperature flux and potential temperature-variance budget equations and the mean momentum and mean potential temperature equations. The scaling of the terms in the budget equations were obtained using both the Monin-Obukhov similarity theory and the Multipoint Monin-Obukhov similarity theory. The small parameters with the most impact in the

perturbation equations are $(-z_i/L)^{-4/3}$, $(-z_i/L)^{-2/3}$ and $-h_0/L$, where z_i , L and h_0 are the inversion height, the Obukhov length and the roughness height respectively. These parameters represent the effects of the mean shear production of the u -variance, the unsteadiness of the inner-outer layer and the buoyancy production of the w -variance on the mean profile. The portion of the mean profile in each scaling layer is expanded asymptotically in terms of these small parameters.

Tong & Ding (2020) have performed asymptotic matching in the two overlapping layers between the three scaling layers, and obtained the leading-order expansions (the local-free-convection scaling and the log law). In the present work, the asymptotic matching between the outer and inner-outer layers to the second order led to the higher-order expansion terms, which account for the deviations from the local-free-convection scaling due to mean shear production of the u -variance and the unsteadiness, a result of finite values of z_i/L . The asymptotic matching between the inner-outer and inner-inner layers results in the higher-order expansions that account for the deviations from the log law due to buoyancy production, a result of finite values of h_0/L .

The asymptotic expansions were used to fit (through linear regression) the set of all the suitable field data, which includes a range of z_i/L and h_0/L values, instead of individual profiles, to obtain the value of U_m/u_* for each profile and the universal expansion coefficients. Using the data set increases the amount of regression data compared with individual profiles, thereby reducing the uncertainties in the regression results. The theoretical prediction shows an excellent agreement with the data set, best seen in figures 3 and 5, indicating that the higher-order effects, i.e. the departures from the leading-order profile are well captured by the higher-order expansions.

We note that because the $-z/L$ values for the profiles are generally larger than 0.1, the leading-order logarithmic profile is hardly directly observable, making a determination of the von Kármán constant very difficult. By fitting the higher-order expansions to the data set, the leading-order profile and the von Kármán constant can be indirectly obtained. The von Kármán constant obtained in the present work (0.344) is close that obtained by Businger *et al.* (1971) (0.35), but is smaller than the values obtained in many field measurements (Högström 1996). However, the previous values were invariably

obtained by fitting the leading-order profile (the log law) to the measured profile, the latter including contributions from the higher-order terms. Since the second-order term is negative (equation (4.2)), such a fit tends to underestimate the leading-order term, and therefore overestimate κ . It would be useful to apply our procedure to a wider range of data to further investigate the issue of the value of the von Kármán constant.

The asymptotic expansions also show that the convective logarithmic friction law derived by Tong & Ding (2020) is valid to at least second order. Therefore, U_m/u_* only depends on L/h_0 and there are no other parameters involved. The friction law shows very good agreement with the data. In contrast, in channel and pipe flows with smooth walls, the logarithmic frictional law is a leading-order approximation (Tennekes 1968; Afzal 1976).

The method of asymptotic expansion quantifies the dependencies of the mean velocity profile on the perturbation parameters and identifies the physical origin of the dependencies, demonstrating its effectiveness as an approach to investigating the ABL. The higher-order mean velocity profile obtained in the present work can achieve higher accuracy over pure empirical profiles obtained through data fitting alone, and could potentially benefit a wide range of applications.

Appendix A. Cross-order matching between the adjacent layers

Here we provide the details of the cross-order matching between the outer and inner-outer layers. Matching the second-order outer expansion with the third-order inner-outer expansion, we have

$$\epsilon_1 U_{o,2} = \epsilon'_1 \epsilon'_3 U_{io,31}. \text{ Thus } \epsilon_1 U_{o,2} = \epsilon_1 z_o^\alpha = \frac{\epsilon_1}{\epsilon'_1 \epsilon'_3} \epsilon'_1 \epsilon'_3 z_{io}^\alpha \left(\frac{L}{z_i}\right)^\alpha, \text{ requiring} \quad (\text{A } 1)$$

$$\frac{\epsilon_1}{\epsilon'_1 \epsilon'_3} \left(\frac{L}{z_i}\right)^\alpha = 1, \quad \frac{u_*}{w_*} \left(\frac{z_i}{L}\right)^{2/3-\alpha} = 1, \quad \alpha = \frac{1}{3}. \quad (\text{A } 2)$$

$$U_{o,22} = D \left(\frac{z}{z_i}\right)^{1/3}, \quad U_{io,312} = D \left(-\frac{z}{L}\right)^{1/3}, \quad (\text{A } 3)$$

Similarly, we match other terms of different orders,

$$\epsilon_1 \epsilon_3 U_{o,31} = \epsilon'_1 U_{io,2} \quad (\text{A } 4)$$

$$\epsilon_1 \epsilon_3 U_{o,31} = \epsilon_1 \epsilon_3 z_o^\beta = \frac{\epsilon_1 \epsilon_3}{\epsilon'_1} \epsilon'_1 z_{io}^\beta \left(\frac{L}{z_i}\right)^\beta \Rightarrow \frac{\epsilon_1 \epsilon_3}{\epsilon'_1} \left(\frac{L}{z_i}\right)^\beta = 1, \frac{u_*}{w_*} \left(\frac{z_i}{L}\right)^{-4/3-\beta} = 1 \Rightarrow \beta = -5/3. \quad (\text{A } 5)$$

$$U_{o,313} = E\left(\frac{z}{z_i}\right)^{-5/3}, \quad U_{io,22} = E\left(-\frac{z}{L}\right)^{-5/3}; \quad (\text{A } 6)$$

$$\epsilon_1 U_{o,2} = \epsilon'_5 \epsilon'_1 U_{io,31} \quad (\text{A } 7)$$

$$\epsilon'_5 \epsilon'_1 U_{io,31} = \epsilon'_5 \epsilon'_1 z_{io}^\gamma = \frac{\epsilon'_5 \epsilon'_1}{\epsilon'_1} \epsilon_1 z_o^\gamma \left(\frac{z_i}{L}\right)^\gamma \Rightarrow \frac{\epsilon'_5 \epsilon'_1}{\epsilon'_1} \left(\frac{z_i}{L}\right)^\gamma = 1, \frac{w_*}{u_*} \left(\frac{z_i}{L}\right)^{-1+\gamma} = 1 \Rightarrow \gamma = 2/3. \quad (\text{A } 8)$$

$$U_{o,23} = F\left(\frac{z}{z_i}\right)^{2/3}, \quad U_{io,322} = F\left(-\frac{z}{L}\right)^{2/3}, \quad (\text{A } 9)$$

$$\epsilon_1 \epsilon_3^2 U_{o,41} = \epsilon'_1 U_{io,23} \quad (\text{A } 10)$$

$$\epsilon_1 \epsilon_3^2 U_{o,41} = \epsilon_1 \epsilon_3^2 z_o^\lambda = \frac{\epsilon_1 \epsilon_3^2}{\epsilon'_1} \epsilon'_1 z_{io}^\lambda \left(-\frac{L}{z_i}\right)^\lambda \Rightarrow \frac{\epsilon_1 \epsilon_3^2}{\epsilon'_1} \left(-\frac{L}{z_i}\right)^\lambda = 1, \frac{u_*}{w_*} \left(-\frac{z_i}{L}\right)^{-8/3-\lambda} = 1 \Rightarrow \lambda = -3.$$

$$U_{o,41} = G\left(\frac{z}{z_i}\right)^{-3}, \quad U_{io,23} = G\left(-\frac{z}{L}\right)^{-3}; \quad (\text{A } 12)$$

$$\epsilon_1 \epsilon_3^2 U_{o,42} = \epsilon'_5 \epsilon'_1 U_{io,313} \quad (\text{A } 13)$$

$$\epsilon_1 \epsilon_3^2 U_{o,42} = \epsilon_1 \epsilon_3^2 z_o^\eta = \frac{\epsilon_1 \epsilon_3^2}{\epsilon'_5 \epsilon'_1} \epsilon'_5 \epsilon'_1 z_{io}^\eta \left(-\frac{L}{z_i}\right)^\eta \Rightarrow \frac{\epsilon_1 \epsilon_3^2}{\epsilon'_5 \epsilon'_1} \left(-\frac{L}{z_i}\right)^\eta = 1, \frac{u_*}{w_*} \left(-\frac{z_i}{L}\right)^{-5/3-\eta} = 1 \Rightarrow \eta = -2. \quad (\text{A } 14)$$

$$U_{o,42} = H\left(\frac{z}{z_i}\right)^{-2}, \quad U_{io,323} = H\left(-\frac{z}{L}\right)^{-2}; \quad (\text{A } 15)$$

$$\epsilon_1 \epsilon_3^2 U_{o,43} = \epsilon'_1 \epsilon'_3 U_{io,323} \quad (\text{A } 16)$$

$$\epsilon_1 \epsilon_3^2 U_{o,43} = \epsilon_1 \epsilon_3^2 z_o^\xi = \frac{\epsilon_1 \epsilon_3^2}{\epsilon'_1 \epsilon'_3} \epsilon'_1 \epsilon'_3 z_{io}^\xi \left(-\frac{L}{z_i}\right)^\xi \Rightarrow \frac{\epsilon_1 \epsilon_3^2}{\epsilon'_1 \epsilon'_3} \left(-\frac{L}{z_i}\right)^\xi = 1, \frac{u_*}{w_*} \left(-\frac{z_i}{L}\right)^{-2-\xi} = 1 \Rightarrow \xi = -7/3.$$

$$U_{o,43} = I\left(\frac{z}{z_i}\right)^{-7/3}, \quad U_{io,313} = I\left(-\frac{z}{L}\right)^{-7/3}. \quad (\text{A } 18)$$

In the similar way, the cross-order matching between the inner-outer and inner-inner layers can be carried out,

$$\epsilon'_1 U_{io,2} = \epsilon'_1 \epsilon''_3 U_{ii,32}, \quad (\text{A } 19)$$

$$\text{Thus } \epsilon'_1 U_{io,2} = \epsilon_1 z_{io}^\alpha = \frac{\epsilon'_1}{\epsilon'_1 \epsilon''_3} \epsilon'_1 \epsilon''_3 z_{ii}^\alpha \left(-\frac{h_0}{L}\right)^\alpha \\ \frac{\epsilon'_1}{\epsilon'_1 \epsilon''_3} \left(-\frac{h_0}{L}\right)^\alpha = 1, \quad \left(-\frac{L}{h_0}\right) \left(-\frac{h_0}{L}\right)^\alpha = 1, \quad \alpha = 1. \quad (\text{A 20})$$

$$U_{io,22} = C' \left(-\frac{z}{L}\right), \quad U_{ii,32} = C' \left(\frac{z}{h_0}\right); \quad (\text{A 21})$$

$$\epsilon'_1 U_{io,2} = \epsilon'_1 \epsilon''_3^2 U_{ii,41} \quad (\text{A 22})$$

$$\epsilon'_1 U_{io,2} = \epsilon_1 z_{io}^\beta = \frac{\epsilon'_1}{\epsilon'_1 \epsilon''_3^2} \epsilon'_1 \epsilon''_3^2 z_{ii}^\beta \left(-\frac{h_0}{L}\right)^\beta \Rightarrow \frac{\epsilon'_1}{\epsilon'_1 \epsilon''_3^2} \left(-\frac{h_0}{L}\right)^\beta = 1, \quad \left(-\frac{L}{h_0}\right)^2 \left(-\frac{h_0}{L}\right)^\beta = 1 \\ \Rightarrow \beta = 2.$$

$$U_{io,23} = E' \left(-\frac{z}{L}\right)^2, \quad U_{ii,41} = E' \left(\frac{z}{h_0}\right)^2. \quad (\text{A 24})$$

Appendix B. Iterative procedure for determining the expansion coefficients

Here we describe the procedure for determining the expansion coefficients for the leading-order term and three higher-order terms for local-free-convection layer,

$$U_o = 1 + \epsilon_1 A \left(\frac{z}{z_i}\right)^{-1/3} + \epsilon_1 D \left(\frac{z}{z_i}\right)^{1/3} + \epsilon_1 \epsilon_3 E \left(\frac{z}{z_i}\right)^{-5/3} + \epsilon_1 \epsilon_3^2 G \left(\frac{z}{z_i}\right)^{-3}, \quad (\text{B 1})$$

$$U_{io} = 1 + \epsilon'_1 A \left(-\frac{z}{L}\right)^{-1/3} + \epsilon'_1 E \left(-\frac{z}{L}\right)^{-5/3} + \epsilon'_1 G \left(-\frac{z}{L}\right)^{-3} + \epsilon'_1 \epsilon'_3 D \left(-\frac{z}{L}\right)^{1/3}, \quad (\text{B 2})$$

The second equation can be written as

$$\frac{U}{u_*} = \frac{U_m}{u_*} + A \left(-\frac{z}{L}\right)^{-1/3} + E \left(-\frac{z}{L}\right)^{-5/3} + G \left(-\frac{z}{L}\right)^{-3} + \epsilon'_3 D \left(-\frac{z}{L}\right)^{1/3}, \quad (\text{B 3})$$

The coefficients A , E , D , G , which are identical for all profiles, and the offset U_m/u_* for each profile are determined through an iterative multi-step procedure.

We first write the mixed-layer defect to include only one higher-order term

$$\frac{U}{u_*} = \frac{U_m}{u_*} + A(-z/L)^{-1/3} + E(-z/L)^{-5/3}, \quad (\text{B 4})$$

For each profile, a planar fit is performed using the liner equation

$$Y = \frac{U_m}{u_*} + A X_1 + E X_2, \quad (\text{B 5})$$

where $Y = U/u_*$, $X_1 = (-z/L)^{-1/3}$, and $X_2 = (-z/L)^{-5/3}$. The intercept from this fit provides an updated U_m/u_* value for the profile.

In the second step, all the profiles are combined and a least-squares fit of the following

equation is performed,

$$\frac{U}{u_*} - \frac{U_m}{u_*} = A(-z/L)^{-1/3} + E(-z/L)^{-5/3} + D\epsilon'_3(-z/L)^{1/3} + G(-z/L)^{-3}, \quad (\text{B } 6)$$

By setting $Y = U/u_* - U_m/u_*$, $X_1 = (-z/L)^{-1/3}$, $X_2 = (-z/L)^{-5/3}$, $X_3 = \epsilon'_3(-z/L)^{1/3}$, and $X_4 = (-z/L)^{-3}$, a linear regression can be performed, providing estimates of the coefficients A , E , D , G .

In the third step, the new values of the coefficients are used to update the U_m/u_* value for each profile. For up to the 10th iteration, U_m/u_* is updated as

$$\frac{U_m}{u_*} = \frac{U}{u_*} - A(-z/L)^{-1/3} - E(-z/L)^{-5/3}. \quad (\text{B } 7)$$

For iterations beyond the 10th, the D and G terms are also included to improve the accuracy

$$\frac{U_m}{u_*} = \frac{U}{u_*} - A(-z/L)^{-1/3} - E(-z/L)^{-5/3} - D\epsilon'_3(-z/L)^{1/3} - G(-z/L)^{-3}. \quad (\text{B } 8)$$

Steps two and three are repeated iteratively until the value of U_m/u_* for each profile converges with the difference between iterations less than 10^{-6} .

The flowchart in figure 10 depicts the iterative procedure used to determine the coefficients.

Appendix C. Ridge Regression for Stabilizing Coefficient Estimation

During the above regression process, it is observed that the parameter D tends to blow up when the higher-order term $(-z/L)^{1/3}$ is small, making the regression problem ill-conditioned. As a result, the least-squares fit may overemphasize small fluctuations in the data by producing unrealistically large values of D . To mitigate this instability, we employed the ridge regression method, which penalizes large coefficient magnitudes. Specifically, the ridge regression method minimizes the following cost function

$$J(\boldsymbol{\beta}) = \|X\boldsymbol{\beta} - Y\|_2^2 + \lambda\|\boldsymbol{\beta}\|_2^2 \quad (\text{C } 1)$$

where

$$X = \left[(-z/L)^{-1/3}, (-z/L)^{-5/3}, (-z/L)^{1/3}, (-z/L)^{-3}, 1 \right]$$

is the data matrix,

$$\boldsymbol{\beta} = [A, E, D, G, \text{constant}]^T$$

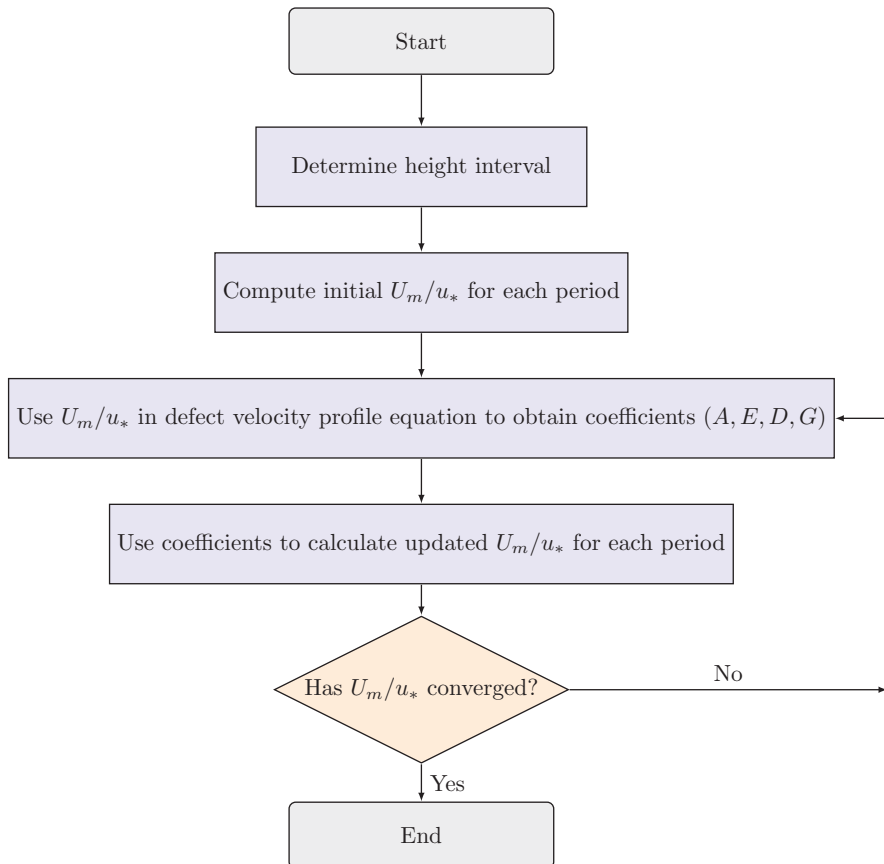


Figure 10: Flowchart of the iterative procedure for determining the coefficients in the Local Free Convection layer

is the coefficient column matrix,

$$Y = \frac{U}{u_*} - \frac{U_m}{u_*}$$

is the response column matrix and λ is the regularization parameter controlling the trade-off between the bias and uncertainties of the estimated coefficients. The analytical solution is given by

$$\boldsymbol{\beta}_{\text{ridge}} = (X^T X + \lambda I)^{-1} X^T Y \quad (\text{C } 2)$$

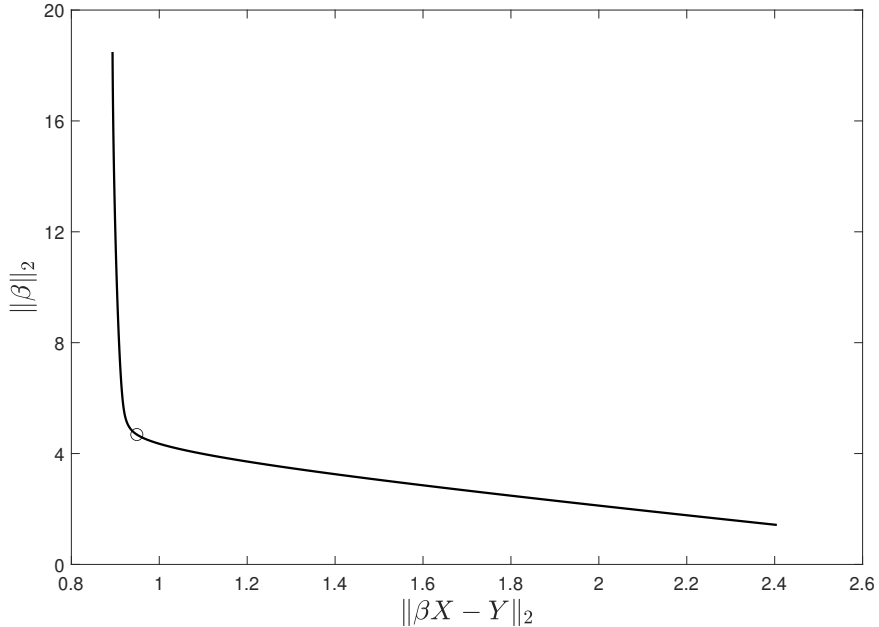
where I is the identity matrix.

To determine the optimal value of λ , we apply the L-curve method, which provides a graphical criterion for optimization. The L-curve is a plot of the solution norm $\|\boldsymbol{\beta}\|_2$ (vertical axis) versus the residual norm $\|X\boldsymbol{\beta} - Y\|_2$ (horizontal axis) for a wide range of λ values (figure 11).

For small λ , the regularization is weak, producing a small residual norm but a large coefficient norm (due to over-fitting) and larger bias. For large λ , the regularization dominates, yielding small a coefficient norm but large residual (due to over-smoothing) and larger uncertainties. The corner of the L-curve, where the curvature is maximum, represents the point of optimal compromise between bias and uncertainty. (Increasing λ further would not significantly reduce the bias but would noticeably increase the uncertainty. On the other hand, reducing λ would not significantly reduce the uncertainty but would significantly increase the bias). Therefore the corner value is selected as the optimal value of the regularization parameter.

Appendix D. Bootstrap-Based Uncertainty Estimation

To assess the statistical uncertainty of the expansion coefficients A, E, D , etc. obtained through regression, we use a bootstrap resampling approach, which does not require an assumption on any particular uncertainty distribution. The approach repeatedly draw samples with replacement from the observed data and recomputes the coefficients for each resampled dataset. The population of the recomputed coefficients are then used (as if they were truly computed from independent datasets) to approximate the sample distribution of the estimators (Hall 1990). In the present work, a total of 2000 resampled datasets are generated. To ensure that each resampled dataset adequately represented the full range of atmospheric stability conditions, the original dataset is first partitioned into three subsets based on the z_i/L . (i) low z_i/L (weekly convective or near-neutral),

Figure 11: L-curve model to determine stabilized λ

(ii) mid z_i/L (moderately convective), and (iii) high z_i/L (strongly convective) regimes. Samples are drawn with replacement from each subset and combined to form a dataset spanning all the stability ranges. This resulted in an ensemble of 2000 samples for each expansion coefficient. The associated uncertainty is quantified by the standard deviation. The bootstrap approach ensures that the estimated uncertainties reflect the combined effects of measurement noise, sensitivity of the fitting procedure, and variability across atmospheric stability ranges.

The resulting bootstrap distributions for the expansion coefficients in the local-free-convection layer and the logarithmic layer are shown in figures 12 and 13, respectively. In the local-free-convection layer, the histograms indicate that the bootstrap realizations are approximately Gaussian. In contrast, the coefficient distributions associated with the logarithmic layer exhibit noticeably skewed and stretched shapes. The bootstrap approach can provide a better estimate of the confidence intervals for these asymmetric distributions.

Expansion coefficients of local free convection layer	A	E	D	G
σ	0.46	0.33	0.09	0.16
95% CI	[-5.20, -3.44]	[-2.16, -0.82]	[0.39, 0.75]	[-0.51, 0.11]
Expansion coefficients of log law layer	κ	C'	$\alpha C'$	h_0
σ	0.02	1.12	0.63	0.008
95% CI	[0.32, 0.39]	[-6.42, -2.24]	[0.40, 2.78]	[0.03, 0.06]

Table 2: Standard deviation and confidence intervals of the expansion coefficients and roughness height

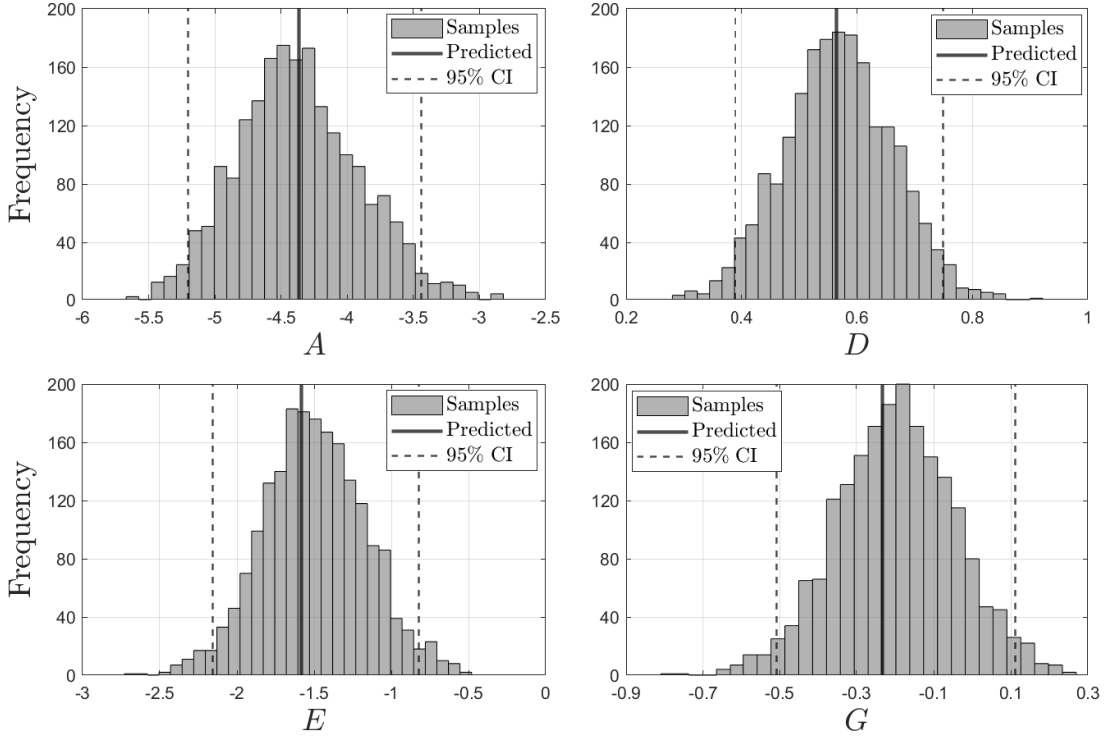


Figure 12: Uncertainty of the coefficients through bootstrap resampling for the local-free-convection layer

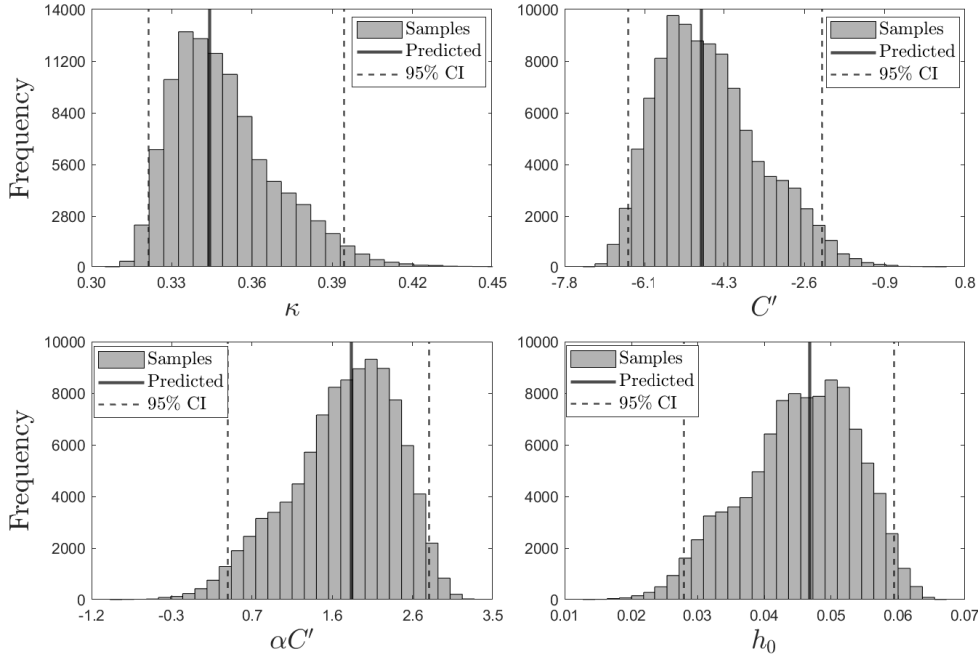


Figure 13: Uncertainty of the coefficients through bootstrap resampling for the Log law layer

REFERENCES

AFZAL, N. 1976 Millikan's argument at moderately large reynolds number. *Phys. Fluids* **19**, 600–602.

ANDREAS, E.L., CLAFFE, K.J., JORDAN, R.E., FAIRALL, C.W., GUEST, P.S., PERSSON, P.O.G. & GRACHEV, A.A. 2006 Evaluations of the von kármán constant in the atmospheric surface layer. *J. Fluid Mech.* **559**, 117–149.

BENDER, C.M. & ORSZAG, S.A. 1978 *Advanced mathematical methods for scientists and engineers*. New York, New York: McGraw-hill book company.

BUSINGER, J. A., WYNGAARD, J. C., IZUMI, Y. & BRADLEY, E. F. 1971 Flux-profile relationships in the atmospheric surface layer. *J. Atmos. Sci.* **28**, 181–189.

VAN DYKE, M. 1975 *Perturbation Methods in Fluid Mechanics*. Stanford, California: The Parabolic Press.

HALL, P. 1990 Using the bootstrap to estimate mean square error and select smoothing parameter in nonparametric problems. *J. Multivariate Anal.* **32**, 177–203.

HOERL, ARTHUR E & KENNARD, ROBERT W 1970 Ridge regression: applications to nonorthogonal problems. *Technometrics* **12** (1), 69–82.

HÖGSTRÖM, U. 1988 Non-dimensional wind and temperature profiles in the atmospheric surface layer. *Boundary-Layer Meteorol.* **42**, 263–270.

HÖGSTRÖM, U. 1996 Review of some basic characteristics of the atmospheric surface layer. *Boundary-Layer Meteorol.* **78**, 215–246.

JOHANSSON, C., SMEDMAN, A., HÖGSTRÖM, U., BRASSEUR, J.G. & KHANNA, S. 2001 Critical test of the validity of monin–obukhov similarity during convective conditions. *J. Atmos. Sci.* **58**, 1549–1566.

KAIMAL, J. C., WYNGAARD, J. C., HAUGEN, D. A., COTÉ, O. R., IZUMI, Y., CAUGHEY, S. J. & READINGS, C. J. 1976 Turbulence structure in the convective boundary layer. *J. Atmos. Sci.* **33**, 2152–2169.

VON KÁRMÁN, THEODORE 1930 Mechanische Ähnlichkeit und Turbulenz. In *Proc. Third Int. Congr. Applied Mechanics*, pp. 85–105. Stockholm.

KAZANSKI, A. B. & MONIN, A. S. 1960 A turbulent regime above the surface atmospheric layer. *Izv. Acad. Sci., USSR, Geophys. Ser.* **1**, 110–112.

KHANNA, S. & BRASSEUR, J. G. 1997 Analysis of Monin-Obukhov similarity from large-eddy simulation. *J. Fluid Mech.* **345**, 251–286.

MONIN, A. S. & OBUKHOV, A. M. 1954 Basic laws of turbulent mixing in the ground layer of the atmosphere. *Trans. Inst. Teoret. Geofiz. Akad. Nauk SSSR* **151**, 163–187.

OBUKHOV, A. M. 1946 Turbulence in the atmosphere with inhomogeneous temperature. *Trans. Inst. Teoret. Geofiz. Akad. Nauk SSSR* **1**, 95–115.

PANTON, RONALD L. 2005 Review of wall turbulence as described by composite expansions. *Applied Mechanics Reviews* **58**, 1–36.

PARLANGE, MARC B & BRUTSAERT, W 1990 Are radiosonde time scales appropriate to characterize boundary layer wind profiles? *J. Appl. Meteorol. Climatol.* **29** (3), 249–255.

PRANDTL, LUDWIG 1925 Bericht über die Entstehung der Turbulenz. *Z. Angew. Math. Mech* **5**, 136–139.

SALESKY, S. & CHAMECKI, M. 2012 Random errors in turbulence measurements in the atmospheric surface layer: Implications for monin–obukhov similarity theory. *J. Atmos. Sci.* **69**, 3700–3714.

TENNEKES 1968 Outline of a second-order theory of turbulent pipe flow. *AIAA J.* **6**.

TENNEKES, H. & LUMLEY, J. L. 1972 *A First Course in Turbulence*. Cambridge, MA: MIT press.

TONG, CHENNING & DING, MENGJIE 2019 Multi-point monin-obukhov similarity in the convective atmospheric surface layer using matched asymptotic expansions. *J. Fluid Mech.* **864**, 640–669.

TONG, C. & DING, M. 2020 Velocity-defect laws, log law and logarithmic friction law in the convective atmospheric boundary layer. *J. Fluid Mech.* **883**, A36.

TONG, C., MAYOR, S.D., ONCLEY, S.P., RODEN, C., BROWN, W.O.J., SPULER, S.M., HAYMAN, M., MORLEY, B.M., WITTE, J., DÉRIAN, P., DE WEKKER, S.F.J., SUN, J., BARSKOV, K. & POURABDOLLAH, D. 2026 Multipoint monin-obukhov similarity theory horizontal array turbulence study ($m^2\text{hats}$). *Bull. Amer. Meteoro. Soc., Early online release*.

WARNER, T. 2010 *Numerical Weather and Climate Prediction*. Cambridge: Cambridge University Press.

WILLOUGHBY, RALPH A 1979 Solutions of ill-posed problems (an tikhonov and vy arsenin). *Siam Review* **21** (2), 266.

WOLFSON, R. 2012 *Energy, Environment and Climate*. New York: Noroton.

WYNGAARD, JOHN C. 2010 *Turbulence in the Atmosphere*. Cambridge University Press.

WYNGAARD, J. C., COTÉ, O. R. & IZUMI, Y. 1971 Local free convection, similarity, and the budgets of shear stress and heat flux. *J. Atmos. Sci.* **28**, 1171–1182.